Landau-Levich flow visualization: Revealing the flow topology responsible for the film thickening phenomena

H. C. Mayer and R. Krechetnikov
Department of Mechanical Engineering, University of California, Santa Barbara, California 93106, USA

(Received 31 May 2011; accepted 28 February 2012; published online 4 May 2012)

An extensive body of experimental work has proven the validity of the analysis of Landau and Levich, who were the first to determine theoretically the thickness of the film deposited by the withdrawal of a flat substrate from a bath of liquid with a clean interface. However, there are a number of experimental investigations that have shown that surfactants in the liquid may result in a thickening of the deposited film. Marangoni phenomena have usually been considered responsible for this effect. However, some careful experiments and numerical simulations reported in the literature seemed to rule out this view as the cause of the observed behavior. Despite all these studies and the number of reports of film thickening, an experimental study of the flow field close to the coated substrate in the presence of surfactants has never been undertaken. In this paper we will present a set of flow visualization experiments on coating of a planar substrate in the range of capillary numbers $10^{-4} \lesssim Ca \lesssim 10^{-3}$ for sodium dodecyl sulfate solutions with bulk concentrations of $0.25\ \text{CMC} \leq C \leq 5.0\ \text{CMC}$ (critical micelle concentration). It was evident during experiments that the flow field near the meniscus region exhibits patterns that can only be explained with a stagnation point residing in the bulk and not at the interface. As opposed to patterns with an interfacial stagnation point, the observed flow fields allow for the increase in film thickness due to the presence of surfactants compared to the clean interface case. © *2012 American Institute of Physics*. [http://dx.doi.org/10.1063/1.4703924]

I. INTRODUCTION

Dip coating, in which a substrate is withdrawn from a bath, is perhaps the oldest and simplest form of liquid film deposition.[1] Although employed in industry to coat objects of various shapes and sizes, scientific investigation of dip coating has typically made use of flat and cylindrical substrates. For the case of Newtonian liquids the thickness of the film $\overline{h}_\infty$ is a function of fluid properties (i.e., surface tension σ, viscosity μ, and density ρ), gravity g, withdrawal velocity U, and substrate curvature r. Dimensional analysis provides a relationship for the relevant parameters of the form[2]

$$\overline{h}_\infty / l_c = f(Ca, Re, Go), \tag{1}$$

where $l_c = \sqrt{\sigma/\rho g}$ is the capillary length, $Ca = \mu U/\sigma$ is the capillary number, $Re = \rho U \overline{h}_\infty/\mu$ is the Reynolds number, and $Go = r/l_c$ is the Goucher number. The question of film thickness for the vertical withdrawal of a flat substrate, $Go \gg 1$, in the limit of small capillary number with no inertia effects was first addressed theoretically by Landau and Levich[3] who arrived at a relationship of the form

$$\overline{h}_\infty = 0.945\, l_c\, Ca^{2/3}. \tag{2}$$

This law holds only for clean interfaces and implies the corresponding flow field near the substrate[4] shown in Figure 1(a). The distinguishing feature of this flow field is a surface stagnation point located $3\overline{h}_\infty$ from the substrate.[5] The first experimental confirmation of the Landau-Levich expression can be attributed to Deryagin and Titievskaya,[6] who coated tubes of negligible curvature using oil for $2 \times 10^{-5} < Ca < 10^{1}$. The coating of thin wires, the formation of thin films on the inside of

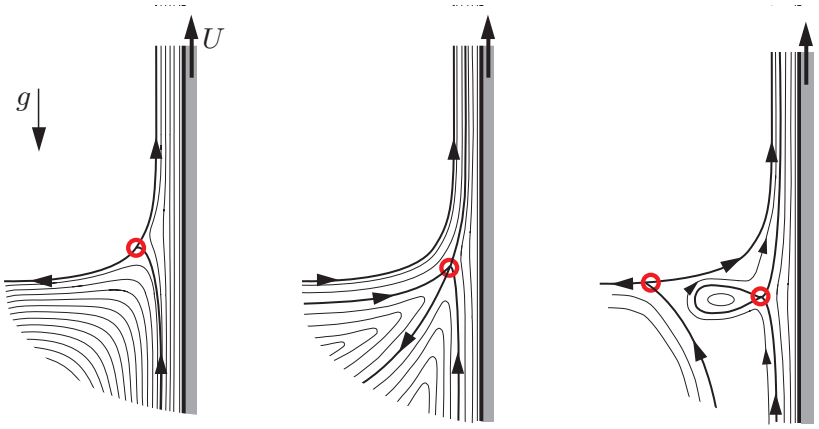

FIG. 1. Various flow fields associated with the Landau-Levich problem: (a) clean and soluble surfactant-laden interface cases[9] with one interfacial stagnation point, (b) surfactant laden interface with one interior stagnation point, and (c) surfactant-laded interface with two stagnation points.[23] Outer phase (air) motion is not shown, but can be inferred from the motion at the liquid-air interface.

capillary tubes by the passage of bubbles (Bretherton problem[7]), and the withdrawal of soap films (i.e., Frankel's law[8]) are considered "sister" problems to the flat plate case of Landau and Levich and possess solutions similar to Eq. (2).[9]

Experimentally observed deviations in the thickness of films predicted by the Landau-Levich equation have been attributed to a variety of reasons including effects of inertia,[10–12] substrate charge and pre-treatment procedures[13,14] (i.e., cleaning[15]), and surfactants.[2,7,16–20] The deviations observed in the presence of surfactants usually correspond to films thicker than predicted by (2). It has become common to represent this effect using the thickening factor α, a ratio of the experimentally measured film thickness to that predicted by Eq. (2),

$$\alpha = \overline{h}_{\infty,\text{measured}}/\overline{h}_{\infty,\text{theory}}, \tag{3}$$

which, in general, can be a function of the capillary number,[7,16] surfactant concentration,[17–19] and the coated object geometry.[17,18] The theoretical film thickness, $\overline{h}_{\infty,\text{theory}}$, which is a function of σ through both the capillary length and capillary number (2), is computed with the equilibrium surface tension σ_{eq} corresponding to the prescribed bulk concentration C with a surfactant uniformly distributed at the interface.

Recent theoretical and numerical studies have attempted to elucidate the mechanisms responsible for film thickening in the presence of surfactants.[9,21–23] Several flow field topologies, cf. Figures 1(a)–1(c), have been proposed which include single stagnation points residing at or below the interface as well as multiple stagnation points. As will be discussed in Sec. V, these studies have not led to a consensus as to the mechanism responsible for film thickening and the conjectured flow fields were not supported by experimental evidence. The authors' opinion is that the true flow topology needs to be determined through direct flow visualization experiments to resolve this long-standing question, as well as a careful survey of the literature is required to address various confusions. As far as the authors are aware, the results of the experiments presented here for the first time resolve the structure of the flow field close to the coating substrate, when surfactants are present, and settle the controversy regarding surfactant effects in the Landau-Levich problem.

The outline of this work is as follows. We begin with a historical review of experimental studies of the Landau-Levich problem in Sec. II, and highlight cases of film thickness measurements (Sec. II A) when surface active impurities were either unintentionally or intentionally added. Attempts at flow visualization of the Landau-Levich problem and similar flows will also be discussed (Sec. II B). In Sec. III, the experimental setup utilized in this study will be detailed (Sec. III A) as will the relevant properties of the surfactant solutions used in experiments (Sec. III C). Results from

the experiments will be presented in Sec. IV along with an examination of relevant length scales (Sec. IV A 1), time scales (Sec. IV A 2), and transient effects (Sec. IV C). A thorough discussion of the observed flow patterns in the context of early reported causes of film thickening (Sec. V A), as well as previous analytical (Sec. V B) and numerical (Sec. V C) studies will be given in Sec. V. The detailed discussion in the latter section serves the purpose of resolving the discrepancies in the literature regarding film thickening in the presence of surfactants and finding a common ground for a wide range of ideas pertinent to this problem. Finally, in Sec. VI, we formulate a number of questions requiring further study.

II. HISTORY OF EXPERIMENTS

In this section we review the relevant history of coating flow experiments, specifically film thickness measurements and examples of flow visualization pertaining to the Landau-Levich problem and "sister" coating flows. While a number of comprehensive review articles on coating flows are available for the interested reader,[24–26] an emphasis is placed here on film thickening in the presence of surfactants.

A. Film thickness measurements

With the exception of the work of Deryagin and Titievskaya,[6] early studies of dip coating from 1922 to 1958 (Refs. 27–30) produced little more than empirical correlations of film thickness or deposited volume for relatively specific applications (e.g., burette dispensing accuracy[28] or calibration of gas meter standards[29]). These studies made use of oils, waxes, and organic liquids possessing relatively large viscosities and low surface tensions compared to water, which makes them less susceptible to adsorption of contaminants. In many cases the fluid properties were not adequately recorded, making direct comparison to later theoretical predictions difficult.[31] Film thickness was inferred by gravimetric techniques, direct micrometer measurements, or photographic means (profiles of thick films on plates and cylinders were photographed). The range of capillary numbers explored in these experiments was $2 \times 10^{-5} < Ca < 2.5 \times 10^{1}$.

The period of 1960–1974, building on the experimental tools and techniques pioneered decades earlier, includes more refined dip coating investigations. A related class of experiments involving the motion of long bubbles through capillary tubes yielded the first real observations of film thickening that can be attributed to surface active impurities. The data of Marchessault and Mason[32] suggested film thickening behavior for air bubbles in aqueous solutions of diglycol laurate, and for benzene and hexane bubbles in water in the $10^{-5} < Ca < 10^{-4}$ range. Bretherton,[7] using benzene and aniline, reported significant variations in the film thickness as compared to theoretical predictions for $Ca < 10^{-5}$. Despite rigorous cleaning methods employed by Bretherton, he conjectured that dissolved impurities could cause "hardening" of the interface (i.e., surface tension gradients allowing the interface to support a viscous tangential stress). But, he concluded on the basis of the magnitude of the predicted thickening that this phenomenon could not account for the observed film thickness deviations.[7]

White and Tallmadge,[33] confirming earlier measurements from experiments on the withdrawal and removal of plates from rinsing baths,[34] reported film thickening by a factor of 1.4–2.0 for the case of dip coating of cylinders with water for $10^{-4} < Ca < 10^{-2}$. The "water paradox," as the authors named the film thickening, was observed for distilled water, as well as combinations of water mixed with pontamine blue dye, sodium chloride, and "Dreft" detergent. The authors claimed that none of these additives produced measurable changes in fluid properties – including surface tension.[35] Gradients in surface tension were disregarded by Tallmadge *et al.* as a possible mechanism for the "paradox" and further study of the effect by Tallmadge and Stella was limited to surface charge and substrate cleaning.[13,14] Later studies[20,36] showed, though, that surface charge and substrate cleaning affect the measurability range[37] of the film thickness and thus lead to the deviations observed by Tallmadge *et al.* In general, however, substrate-liquid interactions yielding an extra body force normal to the substrate may result in substantial deviations from the Landau-Levich law.[36] For example, an attractive interaction potential can produce film thickening. Therefore, it is

inconclusive as to whether surface charge and cleaning can account for *all* of the "water paradox" observations.

Surface impurities were again investigated by Groenveld[2,16] as part of his larger study on dip coating.[2,12,16,38–40] A new optical technique for measuring film thickness was used to demonstrate the effect of the *deliberate* addition of insoluble surface active impurities to the system. By adding drops of hexane and piston oil to a glycerol-water solution, films 1.1–1.8 times thicker than clean interface predictions were observed for $3 \times 10^{-3} < Ca < 3 \times 10^{-2}$. Groenveld speculated that the effect of the impurities, resulting in gradients of surface tension, would enable the surface to sustain a tangential stress. The surface would then move with the same velocity as the substrate and the stagnation point, located at the surface for the clean interface case, would be displaced to the interior of the fluid (cf. Figure 1(b)). This hypothesis was not confirmed through direct measurements.

Analogous to the works of Groenveld,[2,16] Carroll and Lucassen[41] were the first to explore the role of surfactants on film thickening in the course of coating thin wires. For the range $10^{-3} < Ca < 10^{-1}$, film thickness in the presence of the TTAB (tetradecyl trimethyl ammonium bromide) surfactant was nearly 2.5 times that of films produced with clean interfaces. Although the concentration of TTAB was varied, no trend between thickening factor and surfactant concentration was reported.

Between 1974 and 2011, a large body of literature was dedicated to the study of coating flows but only a handful of papers have reported on experiments in which the investigation of film thickening in the presence of surfactants was the focus. Quere, de Ryck, and Ramdane[17,18] performed experiments on liquid coating of fibers from SDS (sodium dodecyl sulfate) surfactant solutions using an amount equal to approximately 8 CMC (critical micelle concentration). Their results confirm film thickening in the range $1.5 \lesssim \alpha \lesssim 2.5$ for $10^{-4} < Ca < 10^{-2}$. The thickening factor was found to decrease with increasing wire radius but remained essentially constant with changes in capillary number. Shen *et al.*[19] extended the work on fiber coating by conducting experiments with different surfactants (anionic, cationic, and non-ionic) and wide ranges in concentration (both above and below the CMC). They observed capillary number invariant thickening, that was highly dependent on surfactant bulk concentration, and explained this complex thickening behavior based on surface remobilization[42] and micelle dynamics. Work on flat substrates was completed by Krechetnikov and Homsy[20] who conducted experiments with glass plates for $10^{-4} < Ca < 10^{-3}$. It should be noted that flat plates exhibit much thicker films as compared to fibers, owing to the difference in characteristic length scale (wire radius r vs. capillary length l_c). The resulting substantial differences in film thickness, owing to the problem geometry, can be responsible for variations in the dominant surfactant transport mechanisms and surfactant availability between plates and fibers for the same ranges of bulk concentration. Using SDS with surfactant concentrations between 0.25–1.0 CMC, Krechetnikov and Homsy reported an average thickening factor of 1.55, although the data show that the thickening factors have a slightly nonmonotonic dependence on withdrawal speed and surfactant concentration. For a large concentration of the highly soluble DTAB (decyl trimethyl ammonium bromide), Scheid *et al.*[22] observed a subtle decrease in thickening factor for flat plates with capillary numbers from 10^{-5} to 10^{-4}, followed by a relatively small thickening factor of 1.06 for $Ca \sim 10^{-3}$.

B. Early attempts at flow visualization

Clearly, film thickness measurements are insufficient to gain a complete understanding of the complexity of a coating flow field in the presence of surfactants. Only direct flow visualization studies can highlight the location of stagnation point(s) and separating streamlines.[1] These characteristic flow features are still points of controversy for the surfactant laden Landau-Levich problem as many speculations regarding the structure of the flow field have been put forth.[9,21–23] Only a small body of work exists pertaining to flow visualization of dip coating[2,30,33,43–46] and no real studies up to this time have probed the surfactant-laden case.

Crude flow visualizations using particles both intentionally and unintentionally placed in the coating fluid were reported by van Rossum[30] for the constant film thickness region, and White[33] for the meniscus region. Van Rossum indicated that the surface moved with a non-zero velocity in the direction of the withdrawal (as opposed to the assumption of Goucher and Ward[27] that the surface should have zero velocity). White also reported behavior consistent with the clean

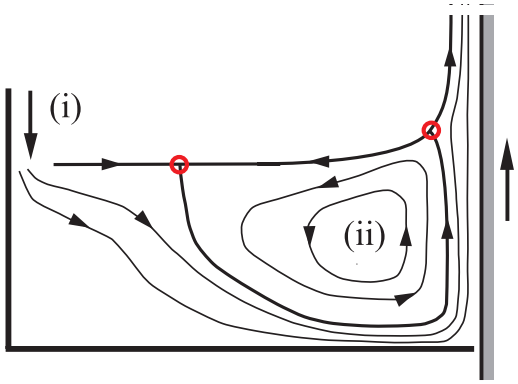

FIG. 2. Qualitative sketch of streamlines for the withdrawal of a flat plate from a small tank as studied by Lee and Tallmadge.[47] The coating liquid was 99% glycerol, resulting in a film thickness ∼2.4 mm. The tank width and height were 65 and 40 mm, respectively. The "feed flux" (i) is the liquid returned to the tank after scraping the continuous belt. Note the location of two surface stagnation points (circles) and the vortex (ii).

interface case – interfacial motion away from a stagnation point toward the bath. Utilizing talcum powder and small bubbles, Groenveld[2] investigated the location of the surface stagnation point and surrounding flow field for thick films of glycerol with clean interfaces and found agreement with theory (cf. Figure 1(a)). No flow visualization for the surfactant laden case was reported in the above-mentioned work. Vortex formation near the meniscus in free coating with a viscous liquid was investigated using dye injection by Lee and Tallmadge[47] in the continuous belt setup. Very little information was given regarding the observed flow field and only a single flow visualization image was provided in their publication. A favorable comparison was made to numerical results, cf. Figure 2 for a sketch of the observed pattern. The vortex was strongly dependent on the nature of the return flow of liquid into the small tank.

The only relatable works that exist with any real detail are those of moving contact line flow visualization.[43,44,46] These studies typically image the flow field near the interface between a solid, an *imperfectly* wetting liquid, and air, which can exhibit a variety of flow patterns including rolling motion (cf. Figure 1(a) but *without* film deposition) and splitting streamlines (both injection and ejection forms),[48] cf. Figure 1(b) but *without* a deposited film. Namely, a split-ejection streamline denotes a streamline within a single fluid phase that separates two regions of the flow field and along which fluid motion is directed away from the contact line.[43,44] Under certain conditions the liquid may be caused to wet the solid surface, resulting in a dip coating pattern (cf. Figure 1(a)). Cerro and co-workers[43,44] used tracer particles to investigate these flow patterns, presumably at low *Ca* numbers as reported in Fuentes and Cerro.[44] For a range of parameters, the flow field was observed to exhibit a typical dip coating pattern with a surface stagnation point (cf. Figure 1(a)). However, an interesting comment was made for a situation when coating was *not* expected and such a typical flow field was not observed, "*A split-ejection streamline was clearly seen ... although there is evidence that a very thin film of oil remained on the glass surface.*"[43] No connection was established by Cerro *et al.* between these observations and coating with surfactants. The high *Ca* withdrawal experiments of Kizito *et al.*[45] using water and Triton surfactant suggested a flow field with a stagnation point at the surface. Their results are far from conclusive owing to lack of detail in the meniscus region. It could be, as we will allude to later (Sec. IV B), that for larger *Ca* numbers it is difficult to interpret the location of the stagnation point for experiments with tracer particles.

Very low *Ca* numbers usually lead to the production of Langmuir-Blodgett (LB) films, i.e., monolayer films of insoluble surfactants deposited on a substrate withdrawn from a trough.[48] These films are typically "dry" in the sense that no water is entrained. The resulting flow pattern during withdrawal should exhibit a split ejection streamline,[48] but without a water film between the monolayer and the substrate. However, recent experiments[46] evidence existence of a split-ejection streamline pattern for a withdrawal speed in excess of the maximum speed for the production of dry films. It is unclear, though, if this pertains to a dip coating (Landau-Levich) regime or if it represents

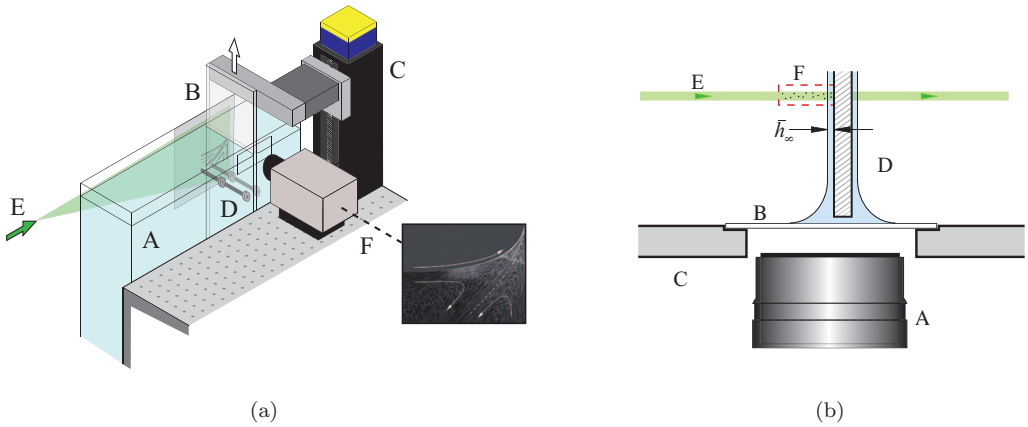

FIG. 3. (a) Experiment setup for Landau-Levich flow visualization with (A) plexiglass tank, (B) glass plate, (C) stepper motor/lead screw, (D) bearings, (E) laser light sheet, and (F) camera. (b) Top down view of coverslip window region of experimental setup with (A) camera lens, (B) glass coverslip, (C) plexiglass sidewall, (D) glass plate withdrawn from tank, (E) laser light sheet, and (F) the region of interest imaged by the camera. The small distance maintained between the glass plate and the coverslip promotes a large capillary rise to aid in non-distorted viewing the flow field within the region of interest (F). This sketch is not to scale.

a transition pattern between the split ejection streamline flow field for dry LB films and that for typical dip coating.[48]

In conclusion, it is evident from a review of the literature that the presence of surfactants leads to film thickening in all known experiments. However, it is also apparent that a complete experimental investigation has never been undertaken to resolve the structure of the flow field close to the substrate for the Landau-Levich problem in the presence of surfactants to explain and fully understand the origin of the film thickening behavior. The sparse results that have been reported in the literature are inconclusive and this warrants the experiments undertaken and reported on in this work.

III. EXPERIMENTAL SETUP AND PROCEDURE

A. Plate withdrawal apparatus

The plate withdrawal apparatus shown in Figure 3(a) was constructed for flow visualization of dip coating. A plexiglass tank, 8 cm × 28 cm × 55 cm (depth × width × height), could accommodate substrates with submerged lengths of up to $L_p = 35$ cm. The dimensions of the tank were sufficient to eliminate any tank wall influence on the meniscus or flow field, a detailed justification of which will follow in the results section (Sec. III D). To improve optical access to the flow field near the substrate, a small window was made using 0.17 mm thick coverslip glass, cf. Figure 3(b). The tank was mounted onto a vibration isolated optical bench during testing. After each experiment the liquid in the tank was drained, the tank was removed from the optical bench, and then thoroughly cleaned. All final rinsing of the tank and any submerged parts was completed with copious amounts of deionized water (18 MΩ cm).

The flat substrates used during experiments were glass strips 6.5 cm wide, 3 mm thick, and 60 cm long. Only $L_p = 35$ cm of that length was coated during experiments, the rest was needed for attachment to the withdrawal apparatus. For experiments with either low surfactant concentration (i.e., 0.25 CMC) or pure deionized water, the glass strips were roughened by chemical etching and sanding with fine grit paper (≥400 grit) to improve wetting.[20] Measurements using an optical profilometer (Veeco Instruments Inc. Wyko NT1100) indicate an average surface roughness of ∼1.1 μm.[49] Controlled substrate withdrawal was performed by a precision stepper motor/lead screw assembly (Velmex BiSlide) providing a range of withdrawal speeds from 0.25–7.6 cm/s. Horizontal deflection and vibration of the substrate were minimized by a set of submerged bearings between which the substrate traveled. The minimization of horizontal deflections serves two purposes. First, reduced vibration provides clear flow field images without distorted streaklines. And second, suppressing vibration limits the effects of normal accelerations (i.e., extra body forces perpendicular to

the substrate) on film thickness variations.[36,50] Unlike a continuous belt setup, removal of a plate from a finite-size bath is accompanied by a decrease in the level of the liquid due to displacement. To eliminate this drop in the free surface level, a compensating plate was devised (not shown in Figure 3(a)): as the substrate was withdrawn, an identical substrate located away from the region of interest was submerged at the same rate.[51]

A thin light sheet was created using a cylindrical lens and a 150 mW, 488 nm argon ion laser (American Laser Corporation), and positioned to highlight tracer particles in a vertical plane at a distance of 30 mm from the coverslip window, deemed sufficiently far to ensure true two-dimensional behavior of the flow field.[1] A Phantom v5.2 camera, with a 55 mm Nikor lens and extension tube set, was used to capture the motion of tracer particles added to the surfactant solutions. A field of view (FOV) of either 8 mm × 6 mm, 12 mm × 9 mm, and 26 mm × 20 mm could be selected and an xyz stage with rotation adjustment provided a means of the camera alignment. It was found that scattered light from the particles was sufficient to produce useful quantitative flow field images. Tracer particles (Polybead® Hollow Microspheres, Polysciences, Inc.) were selected for near neutral buoyancy ($\geq$1.00 g/cm^3), and small size (1 μm). The small size of the tracers is essential to minimize settling during the course of experiments. More importantly, their size must be considerably smaller than the film thickness formed from the withdrawal of aqueous solutions, which are estimated to be within the range of $4\,\mu\text{m} < \bar{h}_\infty < 50\,\mu\text{m}$. The higher-than-water density of the particles was selected to ensure that once placed in the bulk they would not float to the surface and by disrupting the interface would not exhibit surface active behavior (it is known that small particles, if present at the interface and not completely wetted, can act in a manner similar to that of surfactant molecules at fluid-fluid interfaces[52]). Even if some of these particles end up at the interface, which is unlikely due to their density and the presence of surfactants which improve wettability (cf. discussion in Sec. III C), the very low volume fraction of particles ϕ used throughout these experiments ($\phi \sim 10^{-6}$) suggest insignificant effects on the air-SDS solution surface tension.[53]

The overall goal of the flow visualization experiments was to determine the basic structure of the flow field, primarily whether or not a surface stagnation point is present when surfactants are added to the liquid (cf. Figure 1(a)). Thus, knowledge of the detailed velocity field was not needed and no attempt was made to utilize the motion of the tracer particles for particle image velocimetry (PIV) measurements. Exposure times of ~0.05 s provided streak patterns that were more than acceptable in elucidating the flow topology.

The role of transient behavior in the flow visualization results was explored using a modification to the setup shown in Figure 3(a). A compact continuous belt apparatus was constructed that could be placed into the tank in lieu of the glass plate. All components used for imaging (i.e., laser sheet, camera, lens) remained unchanged. The belt, of approximately the same width as the glass plates previously described, was driven by a dc gearmotor at speeds identical to the range of withdrawal velocities tested. Figure 4 shows the continuous belt setup. It was found that the glass plate withdrawal setup produced superior flow visualization images due to reduced vibrations compared to the belt as well as the ability to promote a large capillary rise on the coverslip window (cf. Figure 3(b)).

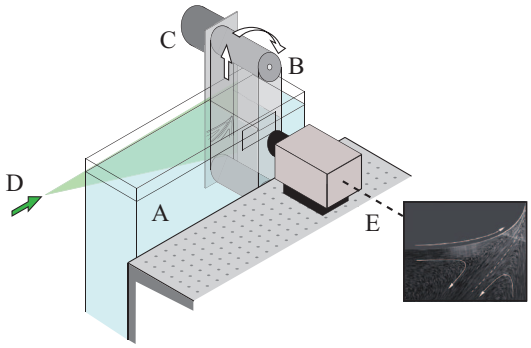

FIG. 4. Continuous belt setup in place of glass plate withdrawal: (A) plexiglass tank, (B) continuous belt apparatus – belt and pulleys, (C) dc gearmotor, (D) laser light sheet, and (E) camera.

TABLE I. Properties of SDS solutions.[56–67]

c (−)	σ_{eq}[a] (mN/m)	μ_s[b] (Pa m s)	κ_s[c] (Pa m s)
0.25	60	$1 \times 10^{-8} - 5 \times 10^{-7}$	$1 \times 10^{-8} - 5 \times 10^{-6}$
0.50	43	$1 \times 10^{-8} - 5 \times 10^{-7}$	$1 \times 10^{-8} - 1 \times 10^{-5}$
1.00	38	$1 \times 10^{-8} - 5 \times 10^{-6}$	$1 \times 10^{-8} - 1 \times 10^{-7}$
5.00	38	$5 \times 10^{-8} - 1 \times 10^{-4}$	$1 \times 10^{-9} - 5 \times 10^{-8}$

[a]Reference 56.
[b]References 60–67.
[c]References 56–59.

B. Procedure

Experiments began by slowly filling the tank with surfactant solution to eliminate the formation of bubbles which could be pinned in the meniscus or pulled into the film – both circumstances adversely influencing the flow field.[54] In all experiments care was taken to clean the tank and all submerged components. But, given the nature of water to easily absorb contaminants, we do not expect that there was a complete absence of surface active impurities. The substrate was then lowered into the tank, passed through the support bearings, and aligned parallel to the front wall of the tank. The space between the edge of the plate and coverslip window, as shown in Figure 3(b), was set as small as possible to promote a large capillary rise on the front window to aid viewing of the flow field.[43,44] Flow in the tank resulting from the setup procedure was allowed to decay before withdrawal was started. After withdrawal, the substrate was returned to its original position by a reversal of the stepper motor. This process was repeated at least twice for each of the five withdrawal speeds. For each speed, movies were filmed with all three FOV settings to record the flow field near and far from the substrate. Frames from all the flow visualization movies were extracted and the particle streak patterns were analyzed using IMAGE J and MATLAB to highlight relevant details of the flow structure. The same procedure was followed for each of the surfactant solutions tested as well as for a pure deionized water case.

C. Surfactant solutions

Sodium dodecyl sulfate (SDS, Fisher Biomedical, 99% purity), a soluble anionic surfactant with a CMC concentration of 8.3 mM and molecular weight of 288.38 g/mol,[20] was mixed with deionized water to make surfactant solutions for the withdrawal experiments. The density of each solution was $\rho = 0.998$ gm/cm^3 and the bulk viscosity $\mu = 1$ mPa s.[55] Table I includes relevant fluid interface properties for the studied SDS solutions, where σ_{eq} is the equilibrium surface tension, μ_s is the surface shear viscosity, and κ_s is the surface dilatational viscosity. Note that the reported ranges of μ_s and κ_s in Table I are based on the current knowledge in the literature, as discussed in detail in the Appendix. Testing was performed in an air-conditioned laboratory where the air temperature remained approximately 20 °C.

SDS was chosen for our experiments because its properties in aqueous solutions have been extensively studied and well characterized. Moreover, previous experimental work on film thickening in the presence of surfactants has made use of SDS[17,18,20] eliminating the need to perform simultaneous film thickness measurements. Concentrations below and above the CMC were used and are reported here in a non-dimensional form using $c = C/C_{CMC}$. SDS mixtures were prepared in quantities sufficient to fill the plexiglass tank, ~12 L. Approximately 60 μL of microsphere solution was added to each mixture. Surfactant solutions were used immediately after preparation. The styrene/acrylic microspheres are supplied in a suspension that contains surfactant needed for stabilization. The amount of this surfactant is negligible compared to the amount of SDS added to make surfactant solutions tested. For example, a 5.0 CMC solution requires the addition of 155.6 gm of SDS to 12 L of water whereas the total weight of the particle suspension is approximately 0.06 gm, of which the stabilizing surfactants constitute a small fraction.

TABLE II. Parameters of SDS transport.[56,69]

Γ_∞[a] (mol/m^2)	D[b] (m^2/s)	k_a[b] (m/s)	k_d[b] (s^{-1})
1×10^{-5}	8×10^{-10}	0.64×10^{-5}	5.9

[a]Reference 56.
[b]Reference 69.

The values of withdrawal speed and the solution properties correspond to capillary numbers in the range of $4.2 \times 10^{-5} < Ca < 2.0 \times 10^{-3}$. These are consistent with the range of capillary numbers in which film thickening had previously been reported.[20] With the possible exception of one set of operating conditions (0.25 cm/s and 0.25 CMC), all tests were performed within the region of measurability of thin films for SDS solutions on glass defined by withdrawal speed and surfactant concentration (cf. Refs. 20 and 37). Performing experiments within the region of measurability ensures that the film deposited on the substrate is stable and will not undergo fast rupture and dewetting from the surface. This also eliminates the possibility that dewetting and drainage into the bath may influence the observed flow patterns. In addition, direct observation of the formation of a stable film was made for each experiment. Typical parameters associated with transport and surface density of SDS are provided in Table II.

The molecular density of surfactant at the interface Γ varies with bulk concentration but is on the order of the maximum surface density Γ_∞ for the range of tested bulk concentrations. Thus, Γ_∞ is employed in the estimates of relevant length and time scales in Sec. IV A. Note that the theoretical value of Γ_∞ reported in Table II comes from a fit[68] of the $\sigma(c)$ data below CMC using the Szyszkowski equation of state, but as noted by Chang and Frances[68] is never achieved and in reality[56] the saturation value is around 3×10^{-6} mol/m^2. The reported diffusivity D and kinetic coefficients k_a and k_d, representing adsorption and desorption respectively, are obtained by conditional averaging of the modified Langmuir-Hinshelwood equation over the entire range of the used concentrations.[69,70]

D. Appropriate tank dimensions

The Landau-Levich equation (2) applies to withdrawal of a continuous substrate from an infinite bath. This mathematical idealization can never be realized in practice, and the effects of tank dimensions on the film thickness and meniscus shape have been a subject of previous studies.[47] The effect of finite tank dimensions (cf. Sec. III A) on the flow field near the substrate was an important consideration here, and steps were taken in the design of the tank to ensure little influence, if any, on the observed patterns.

The height of the tank, $>200\ l_c$, was sufficient to accommodate long substrates and was deep enough to eliminate any influence of the tank height on the flow field and meniscus.[71] The width of the tank, $L_T \sim 100\ l_c$, was originally designed to eliminate crowding of surfactant along the surface with the expectation that the flow field is as shown in Figure 1(a). One can estimate the lower bound on that width in order to eliminate crowding for this configuration: the "residence time" of fluid, $t_{res} \sim L_T/U_S$, moving with surface speed U_S must be greater than the combined time for surfactants to desorb $t_d \sim 1/k_d$ and diffuse away $t_{diff} \sim \eta^2/D$ from the interface; here η is the diffusion length, which can also be thought of as a depletion depth (i.e. the distance from the surface into the bulk that would be required to supply the interface with surfactant). The value of η can be estimated using the surfactant surface and bulk concentrations via $\eta \sim \Gamma/C$ and is $\mathcal{O}(1\ \mu m)$. Therefore, the necessary tank width is given by $L_T > U_S[k_d^{-1} + \Gamma^2/(C^2\ D)]$. For the highest surface speed, on the order of 10 cm/s, and the range of concentrations used the minimum width for the tank is $\sim$2 cm. Thus, the actual width of the tank used in experiments can be judged "infinite" in extent. As has already been reported, the flow field is not that of Figure 1(a) but rather Figure 1(b). Regardless of this fact revealed a posteriori, the width of the tank is still more than sufficient to eliminate any unwanted influence. The depth of the tank, $\sim 30\ l_c$, was sufficient to visualize an undisturbed region 30 mm

from the front window and no significant side flows were observed around the edges of the plate near the tank walls.

IV. RESULTS

A. Characteristic scales in the problem

1. Length scales

The clean Landau-Levich problem is inherently multiscale. Namely, a thin film region characterized by uniform thickness $\overline{h}_\infty$ is connected to a static meniscus region of characteristic dimension l_c. This connection is provided through a dynamic meniscus[9,17,72] of length

$$\lambda \sim l_c\, Ca^{1/3}, \tag{4}$$

this scaling results from a balance between viscous and capillary stresses in that region, i.e., $\mu U/\overline{h}_\infty^2 \sim \sigma/(l_c\lambda)$. For the capillary numbers of interest here this gives the following range of length scales:

$$\overline{h}_\infty = \mathcal{O}(10\,\mu\text{m}) < \lambda = \mathcal{O}(100\,\mu\text{m}) < l_c = \mathcal{O}(1000\,\mu\text{m}).$$

The addition of surfactants to the flow yields further length scales that must be accounted for. One of them is the depletion depth η, which can be thought of as the thickness of a liquid sublayer that is depleted of surfactant in order to pack the surface at equilibrium. This sublayer thickness is a convenient diffusion length and is related to the surface and bulk concentrations as discussed in Sec. III D. As the bulk concentration decreases, the sublayer thickness increases and the role of diffusion becomes more important in the transport of surfactant to and from the interface. It has also been proposed[9,20] based on the theoretical considerations of the balance of interface stretching and surfactant adsorption characteristic times that the addition of surfactant, specifically SDS, may affect the length of dynamic meniscus region, transforming it to $\sim l_c$ compared to Eq. (4). Thus, the surfactant-laden Landau-Levich problem is multiscale with nearly three orders of magnitude separating $\eta \sim \mathcal{O}(1\,\mu\text{m})$ and $l_c \sim \mathcal{O}(1\,\text{mm})$.

Finally, a relevant length scale associated with experimental imaging of the flow field must be called to attention. This is the resolution of the imaging system, l_R, which will vary with camera/lens or objective combination. As an example, in the image shown in Figure 7, each pixel width represents approximately 7 μm. But for situations in which detailed PIV measurements are not required, or when flow structures on the order of $\sim l_c$ are of interest, a resolution closer to $\sim$ 50–100 μm is sufficient. In comparison to the other relevant length scales,

$$\overline{h}_\infty = \mathcal{O}(10\,\mu\text{m}) < l_R = \mathcal{O}(100\,\mu\text{m}) < l_c = \mathcal{O}(1000\,\mu\text{m}).$$

The large span in length scales leads to difficulty in imaging the thin film region and makes resolution of the location of the interior stagnation point ultimately impossible. As a side note, Groenveld[2] was able to visualize the surface stagnation point and the surrounding flow field only for *very* thick films, $\overline{h}_\infty \sim 3$ mm, because of his use of glycerol. In his case $l_R \ll \overline{h}_\infty$, but such thick films are not achievable for aqueous surfactant solutions studied here.

Therefore, the most relevant length scale that will be used to quantify flow field patterns is the capillary length, l_c, which is a key dimension over which the flow field features can clearly be resolved, a distance over which the surfactant surface concentration may vary for SDS solutions as discussed above (i.e., the scale of the dynamic meniscus), and a typical length scale in coating and interfacial flow studies.

Finally, in the context of the discussion of length scales, it is worth commenting on the question of the dynamic meniscus scale (4) vs. l_c (see also the discussion in Sec. IV B 1). We compared the interface shape in the dynamic and static cases for all studied values of the withdrawal speed U and surfactant concentration c, which showed that indeed noticeable difference in the shapes occur in some regimes as exemplified in Figure 5(b) in the case of $C = 5.0$ CMC and $U = 2.54$ cm/s. The accuracy of the present experiments allows one to state with certainty that deviations are present in the parameter region (ii) in Figure 6 characterized by higher withdrawal speeds. The corresponding

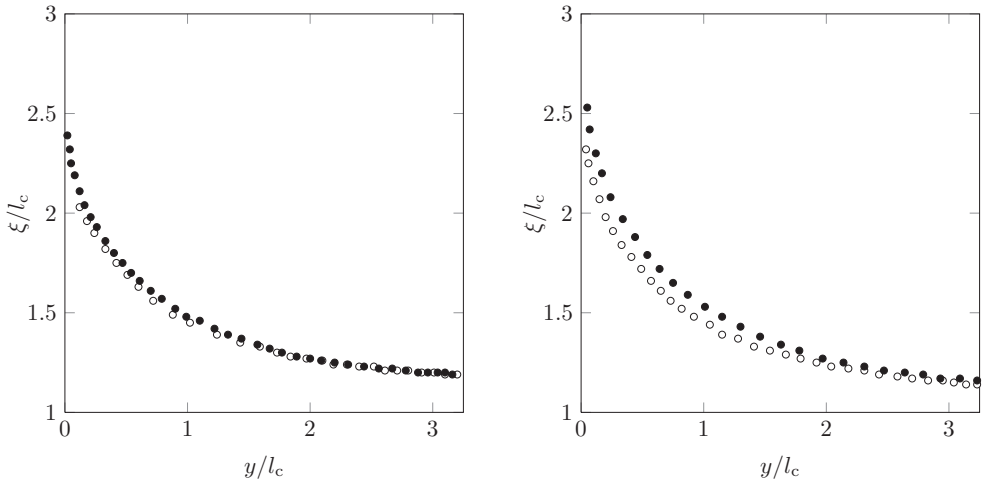

(a) $c = 0.5$, $U = 1.27\,\mathrm{cm/s}$ (b) $c = 5.0$, $U = 2.54\,\mathrm{cm/s}$

FIG. 5. Interfacial profiles extracted from static, ◯, and dynamic, ●, conditions. Symbol size represents the experimental uncertainty of ∼50–100 μm.

range of capillary numbers, $Ca = 10^{-4} - 10^{-3}$, suggests validity of the low capillary number regime and thus unimportance of the inertia effects as discussed in Sec. IV C.

However, in region (i) of Figure 6 the comparison is inconclusive as the interfacial shape variations are comparable with the experimental accuracy. In this context it should be reminded that the goal of the present paper was to visualize the flow structure on scale of the capillary length l_c. As a result, the experimental technique is limited in resolution, e.g., the resolution of the interface on the meniscus scale is on the order of 50–100 μm (even though each pixel only represents ∼7 μm, the particle streaks defining the interface are generally up to ten pixels wide). While with this resolution one can identify the interface profile and compare it to the static one, the result is inconclusive about the dynamic or static nature of the observed meniscus in region (i). This is due to the facts that (a) it is the curvature of the interface which is important when matching the menisci and constructing the solution as follows from the standard Landau-Levich analysis,[3] and (b) the accuracy of the present experiments is not sufficient to resolve curvatures as small variations in the interfacial profile may lead to significant variations in curvature. Therefore, more precise experiments specifically designed to determine meniscus deviations in the presence of surfactants coupled, perhaps, with a technique to

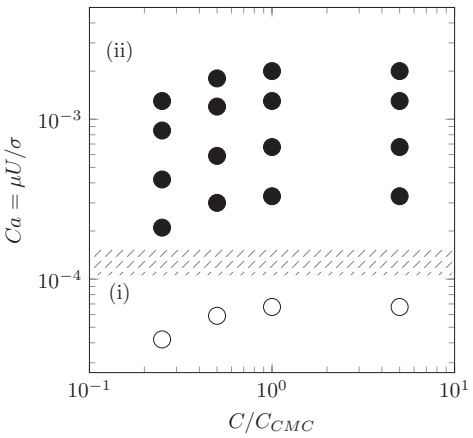

FIG. 6. Observed variation between static interface shape and during withdrawal. Region (ii), ●, indicates conditions for which a readily apparent change in shape exists. No observable change exits in region (i), ◯, given the spatial resolution and uncertainty in our experimental setup.

measure surfactant concentration variations along the interface are necessary to address the question of the scale of the dynamic meniscus, which is beyond the scope of this work.

The above discussion is based on a direct analysis of the experimental data. One should add that based on the ratio of the adsorption time scale $\tau_a \sim \Gamma/(k_a C)$ to that of stretching $\tau_s \sim l_c/U$, i.e., $\tau_a/\tau_s \sim (\Gamma\ U)/(k_a\ C\ l_c)$, one would expect that Marangoni stresses should weaken with (increasing) bulk surfactant concentration. This is contrary to the experimental observations of interfacial shape deviations in Figure 6, which indicate that departures are present even for $C = 1$ and 5 CMC. A possible explanation for this behavior is that the above estimate for τ_a is based on Langmuir-Hinshelwood kinetics and valid for low concentrations, $C <$ CMC, as for higher bulk concentrations (a) the adsorption rate should decrease due to molecular crowding at highly covered interfaces[19] and thus the simple estimate $\tau_a \sim \Gamma/(k_a\ C)$ may be inaccurate, and (b) the micelle formation may increase the time scale of surfactant supply from the bulk to the interface as micelle disintegration requires extra time (see further discussion in Sec. V B 2).

2. Time scales

There are a number of characteristic time scales associated with the development of the flow field as well as surfactant transport in the Landau-Levich problem.

An experimental run time, based on the submerged length of the plate L_p and the speed of withdrawal U, is given as $\tau_{exp} \sim L_p/U$. A small fraction of τ_{exp} is taken up by the acceleration and deceleration of the stepper motor/lead screw assembly.[73] As is expected, the total run time is shortest for the fastest withdrawal experiments (e.g., ~4 s for $U = 7.6$ cm/s), but is relatively long for the slowest withdrawal speeds (e.g., ~130 s for $U = 0.25$ cm/s). Transient fluid motion due to the impulsive starting of a flat plate can be characterized by a timescale associated with the first Stokes problem,[74] $\tau_{St} = \rho\, l_c^2/\mu$ where the characteristic length has been selected as l_c based on the earlier discussion of relevant length scales. This time scale can be used to estimate the onset of fluid motion at the selected distance from the flat plate. Another flow field time scale of interest is associated with stretching or formation of new interface in the meniscus region, $\tau_s \sim l_c/U$.

Film thickening behavior in the presence of surfactants requires knowledge of relevant time scales, that are based on the transport of surfactant to and from the interface. We can separate the transport mechanisms into two categories: diffusion and kinetics. Diffusion is associated with the bulk transport of surfactant due to concentration gradients and the associated time scale is expressed as $\tau_{diff} \sim \eta^2/D$, where η is the relevant diffusion length discussed before and D is the surfactant diffusivity. Surfactant kinetics are associated with the adsorption and desorption of molecules at the interface. Each of the corresponding time scales is given as $\tau_a \sim \Gamma/(C\, k_a)$ and $\tau_d \sim 1/k_d$, respectively. The surface is stretched in the meniscus region, not compressed; therefore adsorption is the only relevant kinetic transport mechanism. The ratio of the adsorption time scale to the diffusion time scale provides a means of estimating which transport mechanism will be limiting. We find that this ratio, given by $\tau_a/\tau_{diff} \sim C\ D/(\Gamma\ k_a)$, is proportional to the concentration. Using the lowest tested concentration (i.e., $c = 0.25$), the ratio of time scales is equal to $\tau_a/\tau_{diff} \sim 25$, which implies that the transport of surfactants is sorption limited for the entire range of concentrations used in experiments.

B. Observed flow topologies

1. Key flow patterns

A typical flow visualization movie frame showing particle streak patterns is provided in Figure 7. The glass substrate is located at the right edge of the image and the direction of travel is toward the top. The need to capture flow patterns on the scale of several millimeters near the substrate implies that the thin film deposited on the glass ($\bar{h}_\infty \sim 10\ \mu$m) cannot be resolved in the upper right corner nor can the exact location of any stagnation point in this thin region. The resolution of the camera/lens combination is equivalent to 7 μm per pixel, which is more than enough to resolve the structure of the flow field indicated by the particle streak patterns. In fact, a resolution of ~ 50–100 μm would be sufficient for our purposes given that PIV measurements were not intended in this study.

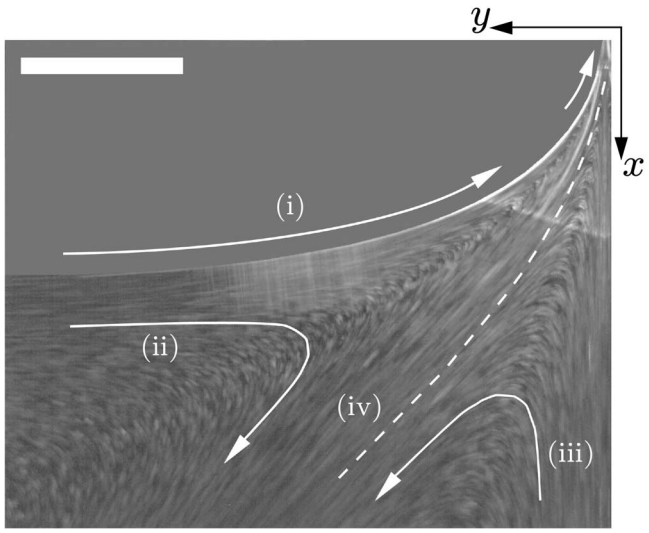

FIG. 7. Typical flow field pattern for $U = 1.27$ cm/s and $c = 0.5$ corresponding to $Ca = 3.0 \times 10^{-4}$. Scale bar represents 2 mm. The small white arrow in the upper right-hand corner indicates that fluid near the surface is swept into the film deposited on the moving substrate.

There are several important features of the flow field that merit description, as they are observed for each of the withdrawal speeds and surfactant concentrations tested. Although not distinguishable in a still image, analysis of the movies clearly demonstrates that the direction of motion of the interface at these scales is directed *toward* the substrate as indicated by (i) in Figure 7. This is contrary to the clean interface case, cf. Figures 1(a) and 10, where the direction of motion of the surface is *away* from the substrate and toward the bath as follows from the classical study of Landau and Levich (in the film region, the free surface in the clean interface case moves upward at the substrate velocity). Figure 8 shows surface velocity distributions $U_S(y)$ along the interface for $c = 0.5$ and 5.0, measured based on particle streaks, i.e., clearly U_S is directed toward the substrate. It is also not surprising though[20] that the surface velocity U_S is of the same order of magnitude as U. Experimental scatter of these distributions suggests that the experimental accuracy is not sufficient to conclude if there is an interfacial velocity variation along the meniscus. Such a scatter is due to the method used to obtain estimates of U_S, i.e., streak lengths produced by particles at/near the surface

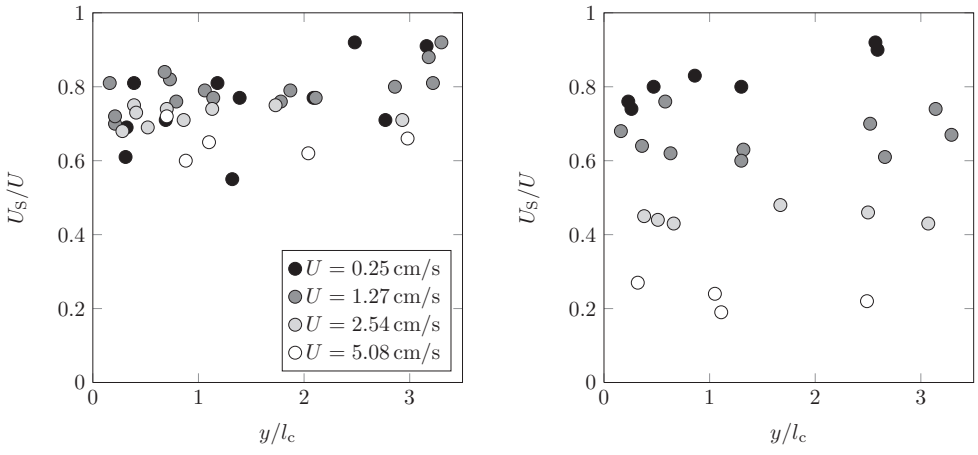

FIG. 8. Surface velocity U_S as a function of interface coordinate y/l_c measured based on particle streak length.

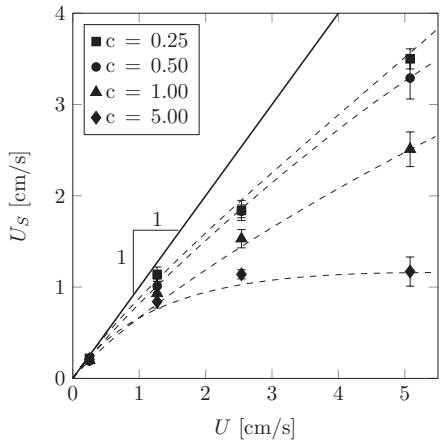

FIG. 9. Surface velocity estimates for the range of studied concentrations, averaged over the values the meniscus region as exemplified in Figure 8. Note that the direction of the surface motion is *toward* the substrate ($U_S > 0$), opposite to the direction for the clean interface case (cf. Figure 1(a)).

with the known exposure for each movie frame. As only very bright and distinguishable streaks can be used (not every particle creates an in focus streak that is distinguishable from others), only a few can be obtained from each movie. Also some streaks are perhaps produced by multiple particles, so that the streak length is the summation of streaks from particles starting at different locations. More detailed PIV measurements, which were not the intention of this work, would be needed for superior determination of surface velocity.

Therefore, in Figure 9 we represent averaging of the interfacial velocity over the meniscus length, which shows non-monotonic dependence of U_S from U as opposed to $U_S = -U/2$ in the clean interface case. It should be noted that even if the interfacial velocity does not vary significantly over the meniscus scale l_c, except for the region near $y = 0$, this does not imply that there are no significant Marangoni gradients in the meniscus region on the scale l_c. Indeed, the interfacial velocity may not vary much, but its gradient in the direction normal to the interface creates substantial viscous stresses which can be maintained only by Marangoni stresses. However, it is clear from Figure 8 that U_S should change from whatever value for a given concentration away from the film to $U_S = 1$ in the film over a short region near $y = 0$; of course, one cannot conclude on the length scale of that region from the given data – it could be on the order of Eq. (4) or different. It is also interesting to observe that interfacial velocity varies substantially with withdrawal speed for $c = 5.0$ compared to $c = 0.5$, which suggests that Marangoni stresses are stronger in the former case as the interfacial velocity varies from lower value in the meniscus region to $U_S = 1$ in the film.

Referring back to the flow field shown in Figure 7, just below the interface there is motion of the liquid toward the substrate and the film (ii), and adjacent to the substrate there is an upward motion of liquid directed toward the film (iii). Not all of this liquid contributes to the formation of the coating film. The liquid that does not become a part of the film is redirected into the bath along a distinct separating streamline (SSL), also referred to as a "split-ejection streamline"[43] in the context of moving contact line studies, shown as the dashed line (iv) in Figure 7. In contrast to the simulated flow fields of Campana *et al.*,[23] there is no stagnation point located at the free surface away from the meniscus region. This observation is confirmed by the flow visualization movies filmed with the largest FOV, as well as direct visual observation of the flow field and interface beyond the FOV of the camera during the course of experiments. Remarkably, the flow pattern in Figure 7 is similar to the case of non-wetting withdrawal when the contact line moves with a prescribed velocity[75] as was mentioned in Sec. II B. However, as was previously pointed out, the combinations of withdrawal speeds and surfactant solutions were all within the range of measurability (cf. Sec. III C) previously determined for SDS solutions,[20] i.e., every experiment resulted in a deposited film on the glass substrate. Thus the observed patterns correspond to the situation when the substrate is perfectly

wetted by the coating fluid – not the situations of a moving solid/liquid/fluid contact line with a finite contact angle[43,75] or the deposition of a LB film.[46]

Without the ability to clearly resolve the precise location of a stagnation point, the features of the flow pattern described above are critical to elucidating the true topology of the Landau-Levich flow field in the presence of surfactants. The possibility of a surface stagnation point is ruled out due to the motion of the liquid surface *toward* the substrate. The presence of the SSL and return flow of liquid toward the bath requires a stagnation point that is located within the fluid. It is apparent that the SSL exists in the upper right corner, cf. Figure 7, to a distance from the substrate within the resolution of our imaging system. Since the stagnation point cannot be located in the constant film thickness region, this suggests that it resides at a location in the neighborhood of the substrate where the film is very thin, which cannot be resolved using our experimental setup. Thus, the only possible topology is that sketched in Figure 1(b). Such a flow field is consistent with the notion that Marangoni stresses, resulting from surface tension gradients, can account for the measured thickening effect. Specifically, the absence of a surface stagnation point allows a *single* Marangoni flow near the surface to entrain fluid that contributes to the formation of the coating film. This is in contrast to the previously reported predictions[4,9] of several competing Marangoni flows near a surface stagnation point that lead to film thinning. The flow topology inferred indirectly here on the scale of $\sim l_c$ has never been experimentally reported as far as the authors are aware and helps one to resolve the controversy in regards to the mechanism of film thickening in the presence of surfactants.

To make the differences between the surfactant-laden and clean flow fields clear, a typical image of the clean interface case is presented in Figure 10. During clean interface experiments the same plate withdrawal setup was used with the only difference being the lack of SDS added to the deionized water in the tank. The experiments were performed immediately after filling the tank with deionized water (i.e., it was not allowed to remain exposed to the laboratory air for extended periods of time), as other studies have shown that "aged" air-water interfaces are easily contaminated[76] with surface active impurities leading to a measurable effect on experimental results.[77] The withdrawal speeds of the plates in Figures 7 and 10 are the same. For the clean interface flow field, note the absence of a separating streamline and the direction of the interface motion as indicated by the arrows. It is apparent that this is the flow field depicted in Figure 1(a).

SDS concentrations below $c = 0.25$ were not explored, primarily because these conditions are outside the measurability range,[20] i.e., film thickness cannot be measured due to strong dewetting effects. Nevertheless, should one ignore the measurability issue, it is expected that a threshold concentration for which the steady flow field transitions from that of Figures 10 to 7 should exist

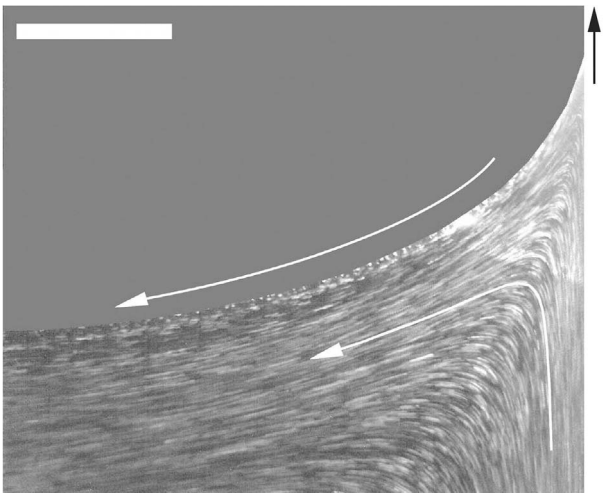

FIG. 10. Flow field pattern for the clean Landau-Levich problem corresponding to $U = 1.27$ cm/s. Scale bar represents 2 mm. The small black arrow in the upper right-hand corner indicates that the fluid near the substrate is carried into the film. Unlike the case shown in Figure 7, liquid from the reservoir surface does not contribute to the film.

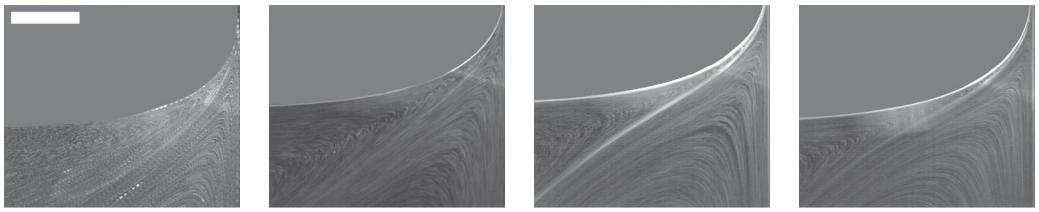

(a) $Ca = 5.9 \times 10^{-5}$ (b) $Ca = 5.9 \times 10^{-4}$ (c) $Ca = 1.2 \times 10^{-3}$ (d) $Ca = 1.8 \times 10^{-3}$

FIG. 11. Change in flow field, specifically separating streamline geometry, for increasing Ca (based on increasing U) at fixed surfactant concentration ($c = 0.50$). The flow field for $Ca = 3.0 \times 10^{-4}$ is shown in Figure 7. Scale bar represents 2 mm.

between $c = 0$ and $c = 0.25$. This is consistent with the abrupt appearance of film thickening at c = 0.1 reported for the coating of wires with SDS solutions.[26] The expected transition in the flow pattern is also hinted at by the structure of the flow field observed at *very* early times for the clean interface experiments, which does in fact evolve between the Figure 7 and 10 patterns. The initially observed SSL structure in the clean interface experiments can be due to inadvertent contamination, by relatively insoluble surface active impurities, that are rapidly swept away from the surface by the motion of the plate.

As in the case of any other bifurcation phenomena, the change in the steady-state flow topology from that in Figure 1(a) to the one in Figure 1(b) happens due to the competition of physical effects (forces). First, the way the flow pattern in Figure 1(a) is formed is as follows: (a) surface tension and gravity are responsible for the (static) shape of the interface; (b) viscous stresses due to moving substrate drag the fluid up, but because of the presence of the static interface, part of the dragged fluid is deflected into the bath thus leading to a stagnation point at the interface where the flow diverges into two parts going into the film and the bath, respectively. Second, once the interface becomes surfactant-laden, Marangoni stresses arise on both sides of the stagnation point. The latter disappears once the Marangoni stresses become strong enough and unidirectional, e.g. for trace amounts of surfactants this can be quantified by the condition $-E\widetilde{\gamma}_s > 2/h$ at each point of the interface following from Equation (34) in Ref. 4 (see also formula (6) below). This happens when the Marangoni flow from the bath towards the film overcomes the counterflow into the bath, 'breaks' the separating streamline, and thus leads to the flow structure shown in Figure 1(b).

2. Separating streamline profiles

An ideal coating flow visualization with surfactant solutions would allow for the capture of all important flow field features: stagnation point location, film thickness, and separating streamline geometry. The thickness of the film ($\mathcal{O}(10\,\mu\text{m})$) and the need to image the flow field far from the front wall ($\mathcal{O}(30\,000\,\mu\text{m})$) makes this task difficult from a technical standpoint. This is especially true given the reflective properties of both the glass plate and the curved air-liquid interfaces (cf. Figure 3(b)).

Therefore, a quantification of the coating flow field in the presence of surfactants should make use of a flow topology that exists on the order of the size of the meniscus, e.g., the SSL shape and position. Future numerical simulations may find such information useful for confirming models. Figure 11 contains four images which represent flow field patterns corresponding to increasing withdrawal speed U (indicated by increasing capillary number) for a fixed surfactant concentration. The most relevant portion of the flow field is the region close to the substrate, within $\sim l_c$ of the upper right corner. What this sequence of images shows is that the SSL approaches the shape of the surface with an increase in withdrawal speed. We suspect that this represents a transition in the flow topology occurring at large capillary numbers, perhaps indicating a decrease in the significance of surface tension gradients.[2]

The sequence of plots in Figure 12 captures the shapes of both the surface (gray) and SSL (white) as withdrawal speed and surfactant concentration vary. Note that due to the changing shape

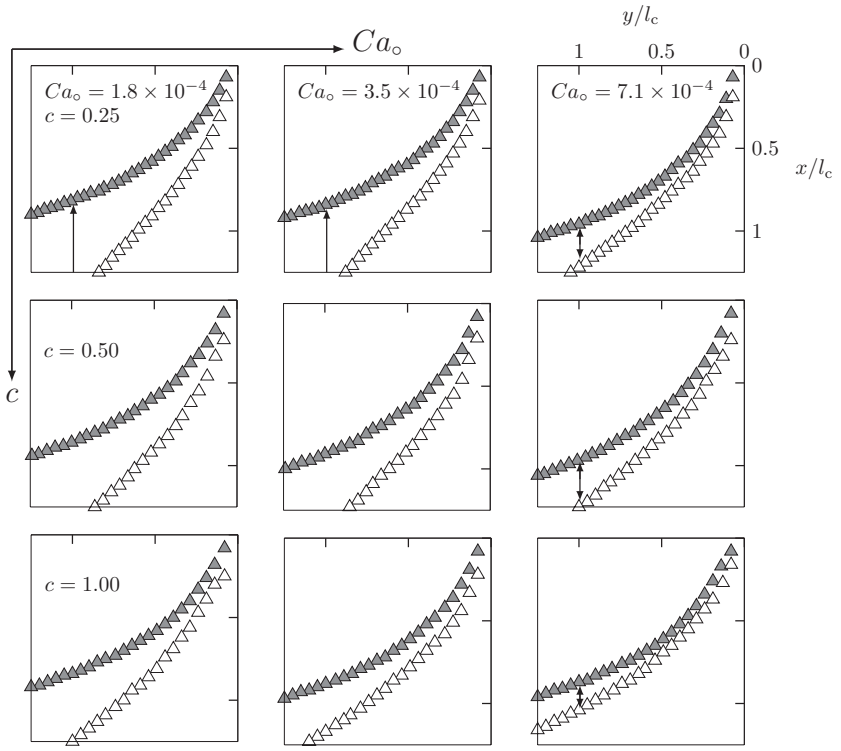

FIG. 12. Variations in surface and SSL shape as a function of the clean interface capillary number $Ca_0 = \mu U/\sigma_0$, used here to isolate only changes in withdrawal speeds U, and surfactant concentration. All vignettes are given on the same scale; orientation of the (x, y)-coordinate system is the same as shown in Figure 7. Since in the clean interface case, $c = 0$, there are no SSLs, they are not presented. The curves of $c = 5.0$ are similar to $c = 1.0$ and have been left out. Only the portion of curves, x/l_c and $y/l_c \leq 1.25$, are shown in each subplot. The vertical arrows in the subplots are included to provide a measure of the relative distance between the surface and SSL curves at $y/l_c \sim 1$ (l_c chosen as a relevant length scale for comparison, see Sec. IV A 1).

of *both* the surface and SSL as functions of these parameters, direct comparisons of only the SSLs would be meaningless. To compare the shapes of the surface and SSL with variations in withdrawal speed in a non-dimensional form without the effect of surfactants, the sub-figures are organized according to Ca_0, the capillary number based on the clean interface value of surface tension σ_0. The data points terminate at $y/l_c \sim 0.1$, which is due in part to the resolution of the images. The comparisons shown in the plots of Figure 12 do not require the precise location of the start of the thin film region to be known so long as the spacing between the surface and SSL is accurate (the error in position is less than the size of the data marks).

The separation distance between the surface and SSL can be measured at any location as can the angle between tangents to the two curves. The most distinguishing trend is the change in shape of the SSL with increasing withdrawal speed (left to right in Figure 12). For any particular surfactant concentration (including $c = 5.0$ not shown in the figure), the SSL approaches the shape of surface with increasing speed. The separation distance decreases and the slopes of the two curves at any chosen x/l_c value become more similar in value. The same type of trend, although not as dramatic, occurs at fixed withdrawal speed but with increasing surfactant concentration (top to bottom in Figure 12). Although we cannot predict what will happen to the SSL for even faster speeds, it is reasonable to assume that it will be more difficult to visualize the SSL and distinguish it from the surface. For large withdrawal speeds and surfactant concentrations (cf. bottom right of Figure 12), the pattern with the surface and SSL being in close proximity could be mistaken for the clean interface pattern (cf. Figure 10) without careful attention to the direction of motion of the surface.

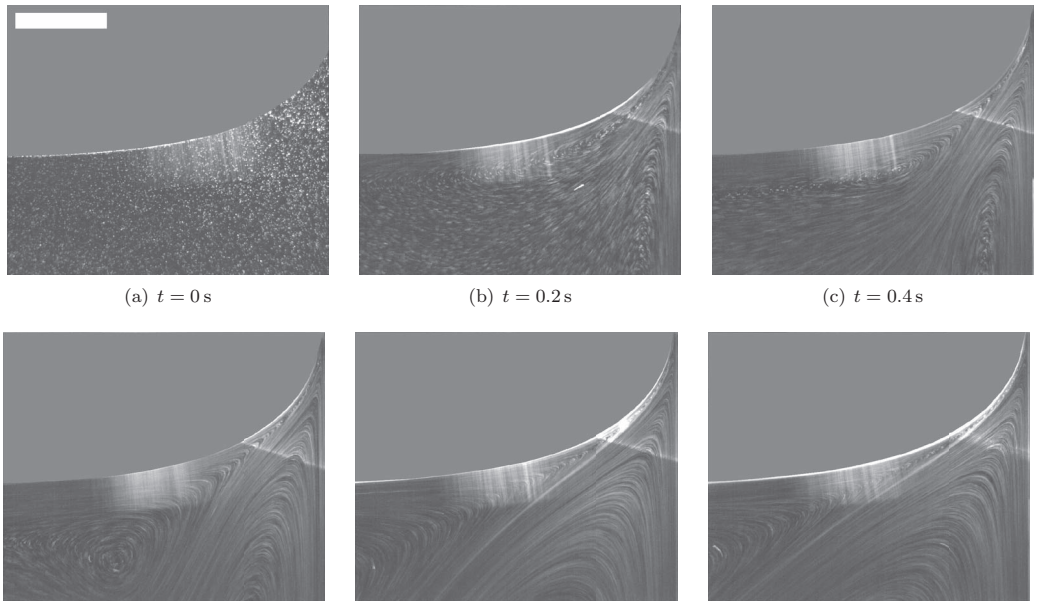

(a) $t = 0\,\mathrm{s}$ (b) $t = 0.2\,\mathrm{s}$ (c) $t = 0.4\,\mathrm{s}$

(d) $t = 0.6\,\mathrm{s}$ (e) $t = 1.6\,\mathrm{s}$ (f) $t = 2.6\,\mathrm{s}$

FIG. 13. Transient motion of the flow field, $t < \tau_{\mathrm{St}}$, for $Ca = 1.8 \times 10^{-3}$ and $c = 0.50$. Scale bar represents 2 mm.

C. Transient and inertial effects

An important question to answer is whether the observed flow patterns, in particular the separating streamline, are the result of the addition of surfactants or caused by transient effects due to the finite withdrawal. We can eliminate transient effects through a series of simple arguments.

Let us start by taking into account the run time τ_{exp} for the experiment compared to the Stokes time scale based on the capillary length. We expect the flow field to be "steady" within $\sim l_{\mathrm{c}}$ of the substrate/meniscus if $\tau_{\mathrm{exp}}/\tau_{\mathrm{St}} > 1$. In the ideal case of an infinite plate and run time, $\tau_{\mathrm{exp}}/\tau_{\mathrm{St}} \to \infty$. Substituting the relations for these time scales into the above ratio results in $(L_{\mathrm{p}}/l_{\mathrm{c}})Re_{l_{\mathrm{c}}}^{-1} > 1$ where $Re_{l_{\mathrm{c}}}$ is the Reynolds number based on the capillary length. For our experiments, given the relatively long plate length, $L_{\mathrm{p}}/l_{\mathrm{c}} \sim 150$. However, $Re_{l_{\mathrm{c}}}$ changes with substrate withdrawal speed and varies between $\sim$10 and 200. This produces a range of $0.75 < (L_{\mathrm{p}}/l_{\mathrm{c}})Re_{l_{\mathrm{c}}} < 15$ and thus, in general, nearly all experiments allow for a steady flow field to establish within l_{c}.

These time scale estimates are supported by flow field images and extracted patterns. For example, Figure 13 shows a sequence of images corresponding to the development of the flow field for $t < \tau_{\mathrm{St}}$. During this time frame, the motion both near and far from the meniscus is changing; however, in panel (f) the SSL has almost established itself. Figure 14 presents the transient behavior of both the surface and the SSL and confirms that the SSL is time-invariant within $x/l_{\mathrm{c}} \leq 1$ of the substrate. But, the motion of the SSL far from the meniscus does change over the course of the experiment. The behavior of the SSL is in direct contrast to the practically time-invariant shape of the entire liquid interface, both near and far from the substrate.

Further confirmation of the steady nature of the observed flow patterns for finite withdrawal experiments, i.e., that typified by Figure 7, came from the results obtained with a continuous belt setup in place of the glass plate withdrawal apparatus, cf. Figure 4. No noticeable difference in the flow patterns were observed using the continuous belt setup (i.e., the SSL was clearly present and maintained a steady position).

The appearance of the Reynolds number $Re_{l_{\mathrm{c}}}$ brings up an important issue regarding inertial effects which have deemed responsible for the film thickening in plate coating.[10] To address this issue we must consider two inertial parameters: the Landau number[78] $La = \rho U^4/\sigma g$ and $Re_{\bar{h}_\infty}$. The Landau number arises from non-dimensionalizing the Navier-Stokes equations for the bulk velocity field, i.e., for the domain on the order of $\sim l_{\mathrm{c}}$. If $La \ll 1$, inertial effects are negligible and the bulk

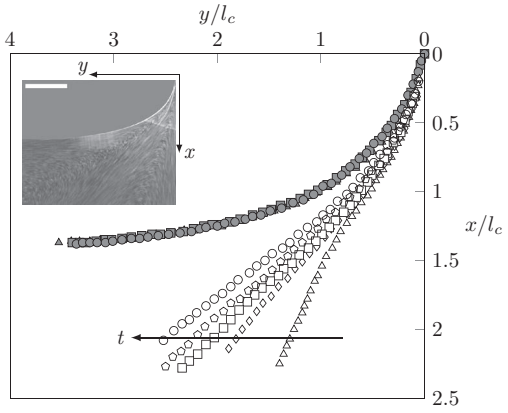

FIG. 14. Transient behavior of the separating streamline for $c = 0.50$ and $Ca = 3.0 \times 10^{-4}$. Shaded data points, of which three sets are plotted, represent the location of the surface which does not change appreciably over the time frame captured here. Open data points represent streamline locations at 1.3 s intervals beginning 0.65 s (△) after start of substrate motion.

flow can be considered a Stokes regime.[9] For the experiments performed, the maximum $La \sim 0.05$ and thus this condition is satisfied. It should be mentioned that, typically, $Re_{\bar{h}_\infty}$ has been used to establish whether inertial effects are significant,[10] and for our experiments $Re_{\bar{h}_\infty} < 1$. But, this is a deceptive parameter in that it does not account for the influence of inertia on the meniscus scale, leading to distortion of the meniscus region and thus of the Landau-Levich law (2). It should be kept in mind that low viscosity liquids can exhibit inertia-related thickening effects even for very low capillary numbers. In fact, there exists a "threshold" capillary number Ca^* for any liquid, above which inertia-related thickening can be significant.[10] For example, for aqueous SDS solutions[10] $Ca^* \approx 2 \times 10^{-3}$, corresponding to $U \approx 16$ cm/s. This value of Ca^* is at the upper range of the experiments performed. Accounting for inertia via $Re_{\bar{h}_\infty}$, clearly not as precise as via La, nevertheless suggests that inertia effects are not the cause of the observed flow patterns.

In conclusion, the flow field for the surfactant-laden case is in stark contrast to the clean interface case as can be seen from the differences between Figures 7 and 10. It is safe to assert that the flow patterns shown in Figure 7 are the result of the addition of surfactants and not due to transient effects associated with the finite size withdrawal setup and/or inertia.

V. DISCUSSION – RELATION TO REPORTED CAUSES OF FILM THICKENING

Experimental analyses aiming to elucidate the mechanism responsible for film thickening have made use of surfactants with different properties,[19] ranges in bulk concentration,[17,19,20] and different coating geometries (i.e., flat plates,[16,20] capillaries, and wires[17,19,41]). These studies relied on film thickness measurements, but not flow visualization or measurements of surface tension/surfactant concentration gradients. Analytical[4,17,79,80] and numerical studies[23,36] have covered a wide range of surfactant transport regimes, surfactant properties, and solution construction approaches – scaling arguments, lubrication approximations, and asymptotic studies, as well as full numerical simulations. As of yet, there is still no real consensus as to the mechanism responsible for film thickening due to the presence of surfactants and even the contradictory result of film thinning has been predicted.[9,81] In what follows we provide a detailed discussion of the relation between the previously reported causes of film thickening and the outcome of the experiments reported here.

A. Early reported causes

The earliest suggested cause of film thickening behavior due to the presence of surfactants can be attributed to Bretherton[7] who noted the "hardening" effect on the interface resulting from surface tension gradients. Applying a rigid surface boundary condition to the bubble interface, a thickening

factor of only $2^{2/3}$ was found. Groenveld[16] too speculated as to the effect of surfactants in the case of dip coating flat plates. As he put it, "*an impure water surface in the pool will expand at the cost of a pure surface in the fresh film...*," that is the driving force due to the surface tension difference between film and bath would give rise to an upward flow at the interface in the meniscus region. His analysis included only an interface moving with the velocity of the flat substrate.[82] A sketch of the corresponding flow field, very similar to Figure 1(b), was provided with almost no explanation of its origin other than being consistent with the assumed surface velocity. Similar qualitative reasoning was echoed by Carroll and Lucassen[41] for the coating of wires, although the thickening factor incorporated by these authors was left as an empirically determined constant.

Despite conjectures regarding the film thickening mechanism, estimates for film thickening factors, and a hypothetical flow field in Groenveld's case, no direct evidence was provided to uncover the true flow field in the presence of surfactants or to determine surface tension gradients which were thought to exist.

B. Lubrication approximations and scaling arguments

1. Surfactant-induced Marangoni effects

When studying the Bretherton problem, Ratulowski and Chang[79] (RC) recognized the need to model the variations in surface tension and surfactant concentration along the interface and in the bulk as the latter are needed to correctly couple the *transport* of surfactant in the bulk phase and along the interface. Using asymptotic analysis RC explored soluble surfactants but restricted their study only to trace amounts ($\sigma/\sigma_c \approx 1$ and $\Gamma \approx \Gamma_c \ll 1$, where subscript c designates quantities at the bubble tip used as a reference value). The typical clean interface scaling for the dynamic meniscus proportional to $Ca^{1/3}$ – was used (see Sec. IV A 1). It was discovered that if bulk concentration gradients exist and adsorption kinetics are fast, then the resulting Marangoni stress due to surfactant concentration variations at the interface can thicken the film and result in a maximum thickening factor of $\alpha = 4^{2/3}$. This limiting factor was found for both $M = 0.1$ and 1.0 where M is the Marangoni number defined as $M = -(\Gamma/\sigma)(\partial\sigma/\partial\Gamma)_\Gamma$. The Marangoni number couples surface tension and surface concentration, and can be thought of as a measure of Marangoni effects on the system. A brief mention by RC of changes in the limiting interfacial velocity of the bubble cap region in the presence of surfactants is provided.[83] Their results suggest that for particular ranges of capillary numbers, this limiting velocity can be of the same sign as the velocity of the surface in the thin film region – indicating that no surface stagnation point exists near the wall. However, no significance appears to be attributed to this possibility and no further indication of changes to the flow field in the presence of surfactants is given. Based on the lack of flow field information provided by RC no comparison to the results of our experiments can be made. Likewise, the capillary tube geometry explored by RC does not even possess a region of the flow field at the $\sim l_c$ scale for which a comparison can be made as the characteristic scale there is the tube radius. Furthermore, RC state[79] that their analysis would not apply to experiments for surfactants at concentrations above the CMC, which were also explored in our experiments.

Around the same time as RC, Park[80] analyzed the Landau-Levich problem for the case of insoluble surfactants, which implies that surface convection and surface diffusion were the only important transport mechanisms. Two regimes were considered, that of small concentrations or trace amounts and small spatial variations in surfactant concentration. Using the method of matched asymptotic expansions and the traditional lubrication approximations in the transition region, the same maximum thickening factor of RC, $\alpha = 4^{2/3}$, was found for both regimes using $0.01 < M < 1.0$ (Ref. 84) despite different transport mechanisms and the insolubility of the modeled surfactant. Park does provide a brief mention of the modified flow field when he comments that the surface stagnation point found in the clean case is "removed" from the surface due to the shear stress resulting from Marangoni effects. This behavior is only reported for one value of the Marangoni number, $M = 0.01$, and it is not clear if such behavior persists for higher values of M or for soluble surfactants. Park does not conclude if the removed stagnation point exists in the liquid, and no further details of the flow field are provided. However, it is clear that hints do exist in the literature[79,80] for the disappearance

of the surface stagnation point in the presence of surfactants beyond the hypothesized flow field of Groenveld. But Park's analysis only applies to the case of insoluble surfactants which is by no means valid for the SDS solutions tested here and elsewhere, and so no direct comparison of the observed flow field patterns can be made. The studies of both Park[80] and Ratulowski and Chang[79] rely on the clean interface scaling (4) of the dynamic meniscus region which, as Krechetnikov and Homsy[9,20] have pointed out, is not always valid and may not apply for the conditions here. This prevents one from performing a local analysis of the problem using standard perturbation techniques and thus questions the relevance of the results of both works[79,80] to the coating experiments presented here, including predictions of the maximum thickening factor and the disappearance of the surface stagnation point. The lack of reported changes to the flow field in the presence of surfactants, beyond comments regarding the surface velocity, can also be attributed to the use of lubrication approximations in these studies. Namely, a key assumption behind the lubrication approximations, i.e. that the flow field is unidirectional, may have prevented the authors from investigating further details of the flow.

Ramdane and Quere[17] (RQ) offered a model for the thickening factor as a function of the properties of the surfactant solution and wire radius b. Their model was predicated on several ideas. First, the surface surfactant concentration Γ varies along the interface from the bath to the film due to convection. In their words, the surface has a "tracting power," due to Marangoni stresses, that varies with the surface velocity. And second, based on earlier predictions[79] the thickening factor should be bound by the limits $1 < \alpha < 4^{2/3}$, where the maximum thickening factor is achieved when the surface velocity is equal to that of the substrate along the entire surface. It should be mentioned that their model was constructed to enforce the upper limit thickening factor and makes use of scaling arguments based on the lubrication approximations for flow in the dynamic meniscus region with the typical scaling $\sim Ca^{1/3}$. However, in the presence of surfactants the dynamic meniscus length was modified to include the effect of the film thickening factor α, i.e., $\lambda \sim b\,\alpha^{1/2}Ca^{1/3}$. To relate the thickening factor to surfactant transport, and ultimately bulk concentration, a relation between the thickening factor and the surface velocity was required. This was accomplished by computing the flux through the dynamic meniscus using an arbitrary surface velocity boundary condition and matching it to the flux though the dynamic meniscus from the clean interface case modified to increase the flux. The result is a difference in surface velocity between the bath and film, ΔU_S, enforcing the condition that the entire interface moves with the velocity of the substrate when $\alpha = 4^{2/3}$ and is given as

$$\Delta U_S = -\frac{1}{2}\left(4 - \alpha^{3/2}\right) U. \tag{5}$$

The relation between thickening factor and the surfactant solution properties is achieved by balancing estimates for the convection and adsorption of surfactant using M as an $\mathcal{O}(1)$ quantity. Convection is based on the surface velocity and dynamic meniscus length scale, while adsorption is related to surface and bulk concentrations using equations that are only valid for "small deviations from equilibrium."

The RQ analysis for the surface velocity varying with the thickening factor yielded limits consistent with earlier works, but this is expected due to the prescribed nature of the solution approach. In fact, the $\Delta U_S(\alpha)$ relationship results in rather interesting behavior. It suggests that increase in the thickening factor corresponds to motion of the surface stagnation point toward the bath, and ultimately at an infinite distance from the substrate when $\alpha = 2^{2/3}$ is achieved. For larger thickening factors, RQ pointed out that the relationship does not predict a surface stagnation point. Rame[21] extended these ideas to track the location of the stagnation point and the flow field streamlines. He conjectured that when the stagnation point disappears from the surface, it reappears within the fluid in the dynamic meniscus and approaches a location halfway between the surface and the substrate for $\alpha = 4^{2/3}$. No explanation for how, or by what means, the stagnation point transitions to the interior was provided.

Recent work on the application of lubrication approximations to coating flows[4] suggests that although the lubrication approximations *can* predict stagnation points and the surrounding flow field, they *cannot* be used to capture behavior too far from the region of applicability. Therefore,

the notion that a surface stagnation point can transition to a region far from the substrate in the model of RQ and extended by Rame is not rigourously justified. For example, the surface velocity $u_{(s)}$ in the case of trace amounts of surfactants, derived systematically by Krechetnikov[4] using the lubrication approximation, is given by (Eq. (34) of that reference)

$$u_{(s)} = \frac{3}{2}\left(1 - \frac{h_\infty}{h}\right) - 1 + \frac{1}{4}E\widetilde{\gamma}_s h, \tag{6}$$

at the location along the interface denoted by the local distance h from the substrate scaled by $l_c\, Ca^{2/3}$, where the Marangoni effects are represented by the last term $E\widetilde{\gamma}_s$. Here $E = -d\sigma/d\gamma|_{\gamma=0}$ is the nondimensional elasticity number and $\widetilde{\gamma}_s = d\widetilde{\gamma}/ds$ the dimensionless surface surfactant concentration gradient with $\widetilde{\gamma}$ being the surface surfactant concentration scaled by $\Gamma_\infty\, Ca^{2/3}$. Equation (6) always predicts the existence of a stagnation point in the vicinity of the substrate and does not allow the surface stagnation point to move to $h \to \infty$ for any surfactant induced behavior. This suggests that the previously discussed relationship between surface velocity and thickening factor of RQ and Rame and flow fields offered by Rame have not been arrived at through systematic means.

A further question is whether the relationship of RQ between the thickening factor and surfactant bulk concentration is valid. First, the surfactant convection time scale is based on the *assumed*, but not justified, dynamic meniscus scaling $\lambda \sim b\,\alpha^{1/2}Ca^{1/3}$. Second, the adsorption flux approximation utilized by RQ is valid only for small deviations in surfactant surface concentration from the equilibrium value. Third, the Marangoni number was evaluated to be $O(1)$ quantity under the assumption that the surfactant concentration is dilute. As RQ pointed out this "*becomes a crude approximation when approaching surface saturation*."

Based on the assumed scaling of the dynamic meniscus and the dilute concentration approximations employed (mimicking the idea of trace amounts of surfactants in earlier works[79,80]), no direct comparison can be made to the experimental results here. The fact that we observe flow fields without a surface stagnation point for corresponding thickening factors of $\sim 2^{2/3}$ can only be considered a coincidence. No experimental evidence exists for the transition of the stagnation point along from the interface for either the wire coating or flat plate geometry.

2. Beyond Marangoni effects: Surface viscosity

Figures 8 and 9 suggest that at small and moderate concentrations, U_s/U is close to one thus indicating large bulk viscous stresses at the interface (keeping in mind that the flow pattern is as shown in Figure 1(b)), while this may not be always the case at the large concentration $c = 5.00$. As known from standard boundary conditions at surfactant-laden interfaces,[85] these bulk viscous stresses at the interface can be supported by both Marangoni and surface viscous stresses. If one assumes that the surfactant-laden interface is Newtonian and thus accepts the standard Boussinesq-Scriven model,[85] which relates surface deformations to surface stresses, then (after the non-dimensionalization based on scaling of the velocity by the withdrawal speed U and coordinates by the capillary length l_c) the effects of surface tension gradients, surface dilatational and shear viscosities are characterized by three non-dimensional parameters,

$$E(\Gamma) = -\frac{\Gamma_\infty}{\sigma_0}\frac{\mathrm{d}\sigma}{\mathrm{d}\Gamma},\ Bq_\mu = \frac{\mu_s}{\mu\, l_c},\ Bq_\kappa = \frac{\kappa_s}{\mu\, l_c}, \tag{7}$$

which are the elasticity number E dependent here on interfacial concentration Γ and two Boussinesq shear Bq_μ and dilatational Bq_κ numbers, respectively. Relative magnitudes of the parameters $E/Ca_0 = (E/Ca)\ (\sigma_0/\sigma_{eq})$ (Ca_0 is the capillary number based on the clean interface value σ_0 of surface tension), Bq_μ, and Bq_κ define the importance of the corresponding effects on the scales defined by (U, l_c) used in the non-dimensionalization. This can be understood with the following (highly simplified) form of the tangential boundary condition:

$$\left.\frac{\partial u}{\partial y}\right|_{y=h} = -\frac{E}{Ca_0}\frac{\sigma_0}{\sigma_{eq}}\frac{\partial \Gamma}{\partial x} + Bq\,\frac{\partial^2 u}{\partial x^2} \tag{8}$$

TABLE III. Values of the elasticity number E for the surfactant concentrations used in our experiments.

E (−)	$c = 0.25$ (−)	$c = 0.50$ (−)	$c = 1.00$ (−)
$(\Gamma_\infty/\sigma_o)(\mathrm{d}\sigma/\mathrm{d}\Gamma)$	0.85	1.00	1.32

in the (x, y) frame of reference shown in Figure 7 and nondimensionalized with respect to the scales defined by (U, l_c). Strictly speaking Eq. (8) just illustrates the balance of the key effects – bulk shear at the interface, Marangoni and surface viscosity stresses – since on the l_c scale and for a curved interface it should be written in the interfacial coordinates and thus have a more complicated form.[85–87]

The elasticity number E measures surface tension gradient effects relative to bulk viscous effects. The factor $\mathrm{d}\sigma/\mathrm{d}\Gamma$ in the elasticity number E corresponds to the sensitivity of surface tension to changes in the surface concentration of surfactant, Γ (note that the negative sign in the definition of E is because $\mathrm{d}\sigma/\mathrm{d}\Gamma < 0$). Values of E can be calculated using knowledge of the behavior of $\sigma(c)$ and $\Gamma(c)$. As this information is readily available for SDS,[56,69] we provide estimates for the values of E based on the Frumkin equation[88] in Table III and, for convenience of the subsequent discussion, capillary numbers in Table IV for each bulk concentration c and plate withdrawal speed U used in our experiments. It can be seen that for the majority of the experiments, the elasticity numbers are on the order of one and suggest the importance of surface tension gradients.

To evaluate the contributions of surface dilatational and shear viscosities measured by the Boussinesq numbers Bq_μ and Bq_κ, respectively, consider the ranges of Boussinesq numbers, Bq_μ and Bq_κ, in Table V and Figure 15 corresponding to the ranges of the surface shear and dilatational viscosities of SDS reported in the literature and summarized in Table I. It is evident that at bulk concentrations below the CMC (i.e., $c = 0.25$, 0.50), the upper limit of Bq_κ is larger than that of Bq_μ. This is consistent with the observation that values of κ_s are typically larger than μ_s for this range of concentrations. At or near the CMC the estimates suggest that Bq_μ and Bq_κ have some overlap in the range of values. We should point out that for concentrations at or below the CMC, the maximum upper limit corresponds to $Bq \sim 5$. For the only SDS concentration above the CMC used in our experiments ($c = 5.00$), the range of Boussinesq numbers based on surface shear viscosity Bq_μ substantially exceeds that for Bq_κ with the upper limit $Bq_\mu \sim 50$.

Singled-out surface viscosity effects (i.e., when surface elasticity can be neglected) were explored theoretically by Scheid *et al.*[22] for moderate capillary numbers, on the order of $10^{-4} - 10^{-3}$, using lubrication analysis and accounting for surface viscosity in the tangential stress balance at the interface, cf. Eq. (8) with $E = 0$. They concluded that film thickening in the absence of Marangoni effects could be explained solely by surface shear viscosity μ_s (or "intrinsic" viscosity) as the dilatational viscosity (or "exchange" viscosity) is expected to be negligible at large surfactant bulk concentrations; in the limit of "infinite" surface viscosity the film thickening factor was found to approach $4^{2/3}$. Flow patterns, specifically the location of the stagnation point, were shown

TABLE IV. Values of the capillary numbers, Ca, for all withdrawal speeds U and surfactant concentrations c used in our experiments.

U (cm/s)	$c = 0.25$ (−)	$c = 0.50$ (−)	$c = 1.00$ (−)	$c = 5.00$ (−)
0.25	4.2×10^{-5}	5.8×10^{-5}	6.6×10^{-5}	6.6×10^{-5}
1.27	2.1×10^{-4}	3.0×10^{-4}	3.3×10^{-4}	3.3×10^{-4}
2.54	4.2×10^{-4}	5.9×10^{-4}	6.7×10^{-4}	6.7×10^{-4}
5.08	8.5×10^{-4}	1.2×10^{-3}	1.3×10^{-3}	1.3×10^{-3}
7.62	1.3×10^{-3}	1.8×10^{-3}	2.0×10^{-3}	2.0×10^{-3}

TABLE V. Estimates of Boussinesq numbers, Bq_μ and Bq_κ.

c (−)	Bq_μ (−)	Bq_κ (−)
0.25	$4 \times 10^{-3} - 2 \times 10^{-1}$	$4 \times 10^{-3} - 2 \times 10^{0}$
0.50	$5 \times 10^{-3} - 2 \times 10^{-1}$	$5 \times 10^{-3} - 5 \times 10^{0}$
1.00	$5 \times 10^{-3} - 3 \times 10^{0}$	$5 \times 10^{-3} - 5 \times 10^{-2}$
5.00	$3 \times 10^{-2} - 5 \times 10^{1}$	$5 \times 10^{-4} - 3 \times 10^{-2}$

by Scheid *et al.*[22] to be affected by surface viscosity through the modified Boussinesq number,[86] $Bq = \mu^*/(\mu\ l_c)$, where $\mu^* = \kappa_s + \mu_s$.[86,87,89] When $Bq \approx 1$, the flow field is similar to the clean interface case, with a stagnation point located at the interface. It is only when $Bq > 25$ that the stagnation point reportedly moves to the interior.

To relate these results to our study, let us look at the conditions when surface elasticity can be neglected (surfactant concentration gradients must be negligible) and thus surface viscosity-induced film thickening may occur. The discussion follows Scheid *et al.*[22] and Krechetnikov and Homsy.[20] The first condition is that the surfactant should be present in the bulk in abundance (concentration should be sufficiently high and film thick enough) to supply surfactant to the interface so that its complete remobilization occurs (i.e., repopulation of the interface resulting in the elimination of surfactant concentration gradients). To quantify this condition consider the interface stretching on some characteristic length l: the number of molecules necessary to fill the interface per unit length in the third dimension is $\Gamma \cdot \eta$ and will be consumed from the sublayer of thickness η near the interface, $C\ l\ \eta = \Gamma\ l$. Accordingly, a sublayer thickness is $\eta \sim \Gamma/C$, which should be much thinner than the film thickness,

$$\frac{\eta}{\overline{h}_\infty} \approx \frac{\Gamma}{C\,\overline{h}_\infty} \ll 1, \tag{9}$$

which is the case for most of the coating conditions in our experiments, except for the lowest speed, 0.25 cm/s, and concentrations $c = 0.25$ and 0.50, in which cases $\eta/\overline{h}_\infty = 1.11$ and 0.52, respectively; however, for SDS at the CMC we get $\eta \sim 1\ \mu$m, while $\overline{h}_\infty$ varies from 4.7 to 45.9 μm with the

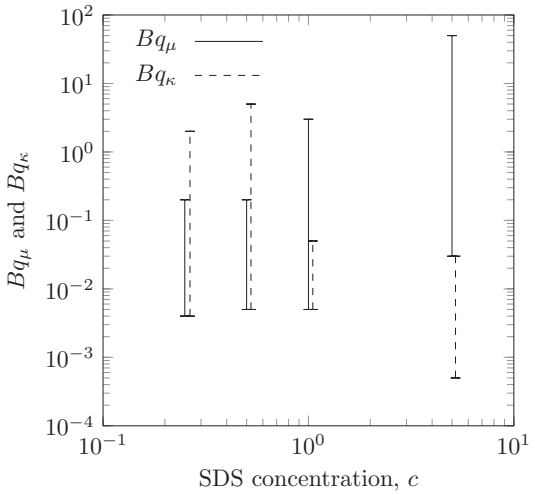

FIG. 15. Plotted values of the ranges for Bq_μ and Bq_κ from Table V to suggest variation in values with concentration. Note that calculated values of both Bq_μ and Bq_κ correspond to the same concentrations c, but to clearly distinguish the two ranges at each concentration (i.e., eliminate overlap that will hide the extent of the dashed lines), Bq_κ values have been translated to the right. As one can observe, the range of values for Bq_μ shifts to higher ones for increasing concentration, but the range for Bq_κ shifts to lower values. At the CMC, both ranges overlap, though there is an apparent drop in the values of Bq_κ.

withdrawal speed changing from 0.25 to 7.62 cm/s. A second condition dictates that there must also be sufficiently fast transport of surfactant from the bulk to the surface compared to the interfacial stretching rate,

$$\frac{\tau_{\mathrm{a}}}{\tau_{\mathrm{s}}} \approx \frac{(\Gamma/k_{\mathrm{a}}C)}{(l_{\mathrm{c}}/U)} \ll 1, \tag{10}$$

where we took into account that interface stretching takes place on the whole meniscus length scale, l_{c}, since there is no stagnation point at the interface as follows from our experimental observations (cf. Sec. IV B 1 and Figure 7). The corresponding adsorption times can be calculated from $\tau_a = \Gamma_\infty/(k_a C)$ based on the Langmuir-Hinshelwood kinetics model and, for the lowest speed of withdrawal 0.25 cm/s, attain values 0.77, 0.46, 0.24, and 0.04 s for the concentrations $c = 0.25$, 0.50, 1.00, and 5.00, respectively;[90] for higher withdrawal speeds the ratio $\tau_{\mathrm{a}}/\tau_{\mathrm{s}}$ only increases. It should be noted that for concentrations above the CMC surfactant adsorption time may be faster than predicted above based on the value of k_a from Table II as the latter was determined using the data only up to the CMC (Ref. 69) and may attain higher value at elevated concentrations.[17] However, above the CMC τ_a may also be affected by the micellar relaxation times:[61,91] the time τ_1 associated with the fast exchange of monomers between micelles and bulk aqueous phase (in the microsecond range) and the time τ_2 associated with micelle dissociation kinetics (in the millisecond range). As τ_1 is faster compared to both the adsorption and stretching times, we are only concerned with the magnitude of τ_2. As follows from Figure 2 in Oh and Shah,[91] at $c = 5.00$ one gets $\tau_2 \sim 0.01$ s, which is comparable to the above predicted adsorption time τ_a, i.e., should the adsorption time be faster based on a more precise value of k_a at concentrations above the CMC, micelle kinetics would delay the adsorption process and thus lead to an increase of the adsorption time scale.

Using the properties of SDS in Table II and for the range of capillary numbers and concentrations explored here, the requirements (9) and (10) are both satisfied simultaneously only for the largest concentration 5.0 CMC, e.g., for the smallest capillary number $Ca = 7 \times 10^{-5}$ we find $\eta/\bar{h}_\infty \sim 5 \times 10^{-2}$ and $\tau_{\mathrm{a}}/\tau_{\mathrm{s}} \sim 5 \times 10^{-2}$. This corresponds to the largest value $Bq \sim 50$ which is in the range of the Bq numbers from Scheid *et al.*[22] for which the flow fields, predicted based solely on surface viscosity effects, are qualitatively similar to those observed in our experiments. Based upon these calculated Bq numbers and their uncertainty, the role of surface viscosity should not be ruled out as a contributing factor in the flow patterns observed in our experiments. For all other concentrations tested in our experiments, the requirements (9) and (10) for neglecting Marangoni stresses are not met.

In addition to the conditions (9) and (10) based upon sorption kinetics considerations, the importance of Marangoni stresses is determined by the material properties of the surfactant-laden interface. Namely, the balance of stresses in the tangential boundary condition (8) should be in favor of surface viscosity contributions compared to the Marangoni effects. There are two key cases to consider – when the meniscus is dynamic of the length scale l_{c} and when the meniscus is dynamic only on the scale (4) as in Scheid *et al.*[22] In the latter case (8) reduces to

$$\left.\frac{\partial u}{\partial y}\right|_{y=h} = -\frac{E}{Ca_0^{2/3}}\frac{\sigma_0}{\sigma_{\mathrm{eq}}}\frac{\partial \Gamma}{\partial x} + Bq\,\frac{\partial^2 u}{\partial x^2}. \tag{11}$$

As one can learn from the values of E and Ca reported in Tables III and IV, respectively, in both cases (8) and (11), Marangoni effects dominate for concentrations $c = 0.25$, 0.50, 1.00, while for $c = 5.00$ the elasticity number is not available[92] thus again leaving the question on the contribution of surface viscosity open. One would expect, though, that should the film thickening mechanisms switch from Marangoni-driven at low concentrations to the one due to surface viscosity at higher concentrations, the film thickening factor should change. This hypothesis requires a separate study as the film thickening data are not available above CMC for coating of flat substrates with SDS solutions.

In conclusion, it must be noted that the wide ranges of μ_{s} and κ_{s} values, their variation with surfactant concentration, and strong dependence of surface tension on the surface concentration

indicate that the surface rheology is quite complex and not fully understood in even such a simple coating flow as the Landau-Levich problem.

C. Numerical simulations

In addition to the theoretical works relying on scaling arguments and lubrication approximations discussed above, the Landau-Levich problem in the presence of surfactants has been studied using numerical simulations (the Bretherton problem has also been approached in this manner). These studies fall into two categories: (a) simulations involving parameters (e.g., surfactant concentration) that differ from those typical of dip coating and involve imposed boundary conditions similar to the clean interface case flow structure,[9] and (b) attempts to simulate[23] with parameters directly relevant to the experiments reported in this work.

A numerical study of the role of soluble surfactants in the Landau-Levich problem was undertaken by Krechetnikov and Homsy[9] (KH) who concluded that the application of standard perturbation techniques to the solution of the problem was inappropriate due to the scaling of the dynamic meniscus for typical coating conditions, i.e., surfactant concentrations close to the CMC require that the dynamic meniscus and the gradients in surfactant concentration scale as $\sim l_c$ instead of $\sim l_c Ca^{1/3}$ given by Eq. (4), which comes from the clean interface case. The motivation for their work was to address the lack of convincing theory and corroborating experimental evidence that Marangoni effects are responsible for thickening. KH used a boundary integral method to model the flow in the Stokes regime ($La \ll 1$) with boundary conditions for the far field corresponding to the reversed solution of Moffatt[93] for a flat plate drawn into a viscous fluid (cf. Figure 1(a)). Their solution approach demonstrated excellent agreement with Eq. (2) for clean interfaces. Insoluble surfactants were found to have no influence on the film formation due to the nature of the prescribed flow field, which is similar to the clean interface case (cf. Figure 1(a)) and thus removes surfactant from the meniscus region. Soluble surfactants with constant bulk concentration in the thin film region (consistent with estimates that $\eta/\bar{h}_\infty \ll 1$) were also considered. Film thinning ($\alpha < 1$) was predicted for $Ca \sim 10^{-2} - 10^{-3}$ in contrast to earlier experimental work.[20] The results of KH are not necessarily relatable to the results of the current experiments given the values of the parameters explored by the authors which are not consistent with the experimental conditions here. Also, there is a dramatic difference in the flow field structures – the numerics of KH relied on a flow field similar to the clean interface case with a surface stagnation point, cf. Figure 1(a), while we observe a separating streamline and surface motion inconsistent with this picture, cf. Figure 1(b).

Recently, Campana *et al.*[23] performed numerical simulations of the full hydrodynamics problem for the flat plate case with soluble surfactants, represented by the properties of SDS from previous studies.[20,69] The range of parameters relevant to surfactant transport was similar to actual coating conditions used in experiments.[20] The numerical results for film thickening factors were reportedly in good agreement with published experiments[20] in the range of $10^{-4} < Ca < 10^{-3}$ with average $\alpha \sim 1.7$ only 8.5% higher than the experimental average.[20] Furthermore, the simulated structure of the flow field for two surfactant concentrations ($c = 0.5$ and 1.0) were provided. They suggest that an interior stagnation point is present along with a surface stagnation point far from the substrate, cf. Figure 1(c). The location of the surface stagnation point changes with bulk concentration, moving further from the substrate with increase in concentration. The results of the study of Campana *et al.* are in question, though, for a variety of reasons. First, the resolution of the grid along the interface is too low, with ~750 points. However, as discussed in Sec. IV A 1, the problem is inherently multiscale and would require a grid resolution on the order of 10^5 to adequately resolve the details of the flow field occurring over the wide range of length scales between 10 $l_c \sim 10^{-1}$ m for the bath geometry, $\sim 10^{-5}$ m for the film thickness, and $\sim 10^{-6}$ m for the sublayer thickness $\eta = \Gamma_\infty / C_{cmc}$ (an indicator of the surfactant diffusion length). Second, the flow field predicted with two stagnation points (cf. Figure 1(c)) is unrealistic and from a dynamical systems standpoint is structurally unstable:[94] the results of our experiments confirm the unrealistic nature of the flow fields. For all of the surfactant solutions used in the experiments reported here ($0.25 < c < 5.0$), although the separating streamline structure hints at the existence of an interior stagnation point, in none of the cases were a surface stagnation point and a corresponding "swirl" pattern observed.

As follows from the above discussion, there is a gap between numerical and experimental understanding of the Landau-Levich problem in the presence of surfactants, which requires development/application of sufficiently accurate numerical approaches to resolve the wide range of length scales and the complexities of surfactant effects for the parameter values relevant to dip coating experiments. This, in particular, is important to achieve reliable predictions of flow topologies observed in experiments. Conceivably, variations in surfactant properties may lead to different flow topologies in analogy with the different flow structures predicted near moving contact lines based on changes in contact angle and viscosity ratio by Huh and Scriven.[75]

VI. CONCLUSIONS

The results of the Landau-Levich flow visualization presented in this work suggest that the dip-coating with the soluble ionic surfactant SDS under the conditions when the transport of surfactant is sorption limited and in the low capillary number regime, has the flow topology that can only be explained with a stagnation point residing in the bulk and not at the interface. Such a flow field allows Marangoni stresses to be the mechanism responsible for the increase in film thickness over that predicted by the Landau-Levich law.

Since here we studied only one well-characterized surfactant, SDS, an interesting question is whether the flow structure depends on the variation of surfactant properties such as the nature of surfactant – ionic vs. nonionic – and different transport conditions – diffusion- vs. sorption-limited. Also the role of surface viscosity over that of surface elasticity in setting up the flow structure requires further investigation as was pointed out earlier by Scheid *et al.*[22]

Therefore, further efforts to investigate the Landau-Levich problem in the presence of surfactants would require both experimental and theoretical approaches:

(a) On the theoretical side, detailed full numerical simulations of the coating flow with sufficient resolution to capture all aspects of the bulk flow and surface flow fields are required along with proper modeling of bulk and surface surfactant transport mechanisms. Such efforts are required because it has been recently proven that the lubrication approximations developed in the past are insufficient for quantitative studies.[9]

(b) On the experiment side, confirmation of numerical simulations can only be expected from detailed PIV measurements applied in the bulk and at the surface in the $\sim l_c$ distance range of the substrate/meniscus. Also, determining the scale of the dynamic meniscus – l_c vs. $l_c\ Ca^{1/3}$ – would require more accurate interface shape and interfacial velocity measurements. In addition, identifying the precise location of the interior stagnation point would be ideal, but this would require a micro PIV at macro distance approach to determine the structure of the flow field in such a thin film region far from any tank sidewalls. To clarify the contribution of surface elasticity to the film thickening phenomena, direct visualization or measurement of surfactant concentrations gradients both at the surface and in the bulk will be required, possibly using tagged or fluorescent surfactants.[95] And to complete the picture, accurate measurements of both the surface shear and surface dilatational viscosities would be necessary to understand the role of these surface rheological effects in the Landau-Levich problem.

Such theoretical and experimental studies would have an impact beyond the academic nature of typical studies of the Landau-Levich problem and provide insight into industrial coating flows with complex fluids.

ACKNOWLEDGMENTS

The authors would like to thank Professor Carl Meinhart for the helpful discussions on the experimental aspects of the project and Professor Homsy for kindly reviewing an early draft of the paper. H.C.M. would also like to thank Bob Hill at UCSB for supplying deionized water used in our experiments. This work was partially supported by the National Science Foundation (NSF) CAREER award under Grant No. 1054267 and American Chemical Society (ACS) Petroleum Research Fund under Grant No. 51307-ND5.

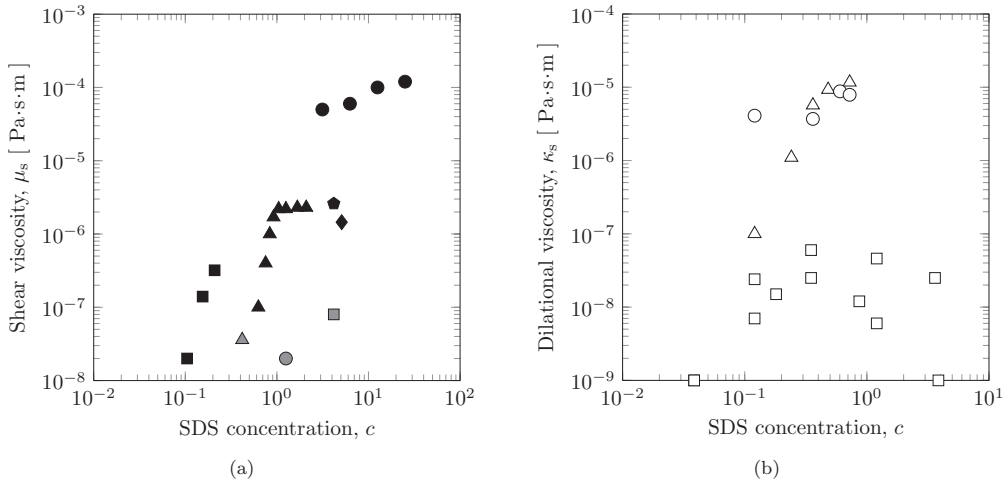

FIG. 16. (a) Surface shear viscosity μ_s data from the literature[97] for a range of SDS surfactant concentrations. Black symbols represent measurements from experiments involving deep channel viscometers, rotating viscometers, and the drag of small objects on the surface. Gray symbols represent inferred values of μ_s (from film or Plateau border drainage). The most complete data sets corresponding to the range of SDS concentrations of interest are those of Poskanzer and Goodrich[62] (▲) and Patist *et al.*[61] (●). (b) Dilatational viscosity κ_s data from the literature for a variety of SDS surfactant concentrations. Symbols correspond to the following sources: (△) Fruhner *et al.*,[58] (◯) Wantke *et al.*,[59] and (□) Kao *et al.*[57] Results from a variety of experimental methods are plotted including the use of oscillating bubbles[58,59] and the maximum bubble pressure[57] methods. Note that, despite the scatter, there appears to be an increase in κ_s with surfactant concentration below the CMC ($c < 1$). With further increase in c the magnitude of κ_s decreases sharply.

APPENDIX: SURFACE VISCOSITIES OF SDS SOLUTIONS

In this section we summarize the values of surface shear μ_s and dilatational κ_s viscosities as functions of the surfactant bulk concentration based on the current knowledge in the literature. Plots of the data are included to suggest concentration dependent trends and to emphasize the scatter in the reported values. Although there are numerous reports in the literature of measurements of surface viscosity of SDS solutions, criteria were established here to select only the most relevant values. Aside from considering values pertaining to the neighborhood of SDS surfactant concentrations used in our experiments, results in which it was ambiguous as to what type of surface viscosity – shear vs. dilatational – was measured were not included.[96]

Surface shear viscosity. Experimental methods used to measure surface shear viscosity are based on the deformation of the surface shape without appreciable change in the area of the surface, i.e., an ideal setup would involve a surface flow with no dilatational motion.[85] Techniques that have been used to explore SDS surface shear viscosity include the deep channel surface viscometer,[60,61] rotating wall viscometers,[62] and the measurement of the drag of small objects such as rotating disks or translating spheres on the surface under investigation.[63,64] Other investigators have inferred values of the surface shear viscosity from the drainage of thin liquid films and Plateau borders.[65–67] A recent review by Stevenson[97] summarizes the measurements of surface shear viscosity for aqueous SDS systems from a variety of experimental techniques and covering a wide span of surfactant bulk concentrations. The data from that review, obtained from eight sources,[98] are shown in Figure 16(a).

Several features regarding this body of experimental values for μ_s should be mentioned. First, it is evident that there is a wide spread in reported values of μ_s at any particular bulk concentration. Part of this discrepancy, as pointed out by Stevenson,[97] is due to the nature of the invasive versus non-invasive (inferred) measurement techniques and the other part is natural scatter due to experimental accuracy. Second, for the sets of measurements with varied surfactant concentration,[61,62] the values of μ_s are seen to increase with concentration and then essentially plateau. The rather abrupt rise was found to occur below the CMC in the experiments of Poskanzer and Goodrich.[62] Their data, measured with a rotating wall knife edge viscometer, also indicate that μ_s is essentially unchanged,

$\sim 2 \times 10^{-6}$ Pa s m, for concentrations in excess of the CMC. Data of Patist *et al.*,[61] measured using a deep channel viscometer, suggest an approximately constant value of μ_s ($\sim 10^{-4}$ Pa s m) for SDS concentrations well in excess of the CMC ($2 \lesssim c \lesssim 20$). Despite trends being qualitatively consistent with each other and each of the techniques highly regarded,[85] the magnitudes of the measured values of μ_s in the plateau region of Poskanzer and Goodrich[62] and Patist *et al.*[61] are in disagreement.

Inspection of the entire group of data points suggests that there is a concentration dependence of surface shear viscosity, with a monotonic increase in μ_s below the CMC.[85] However, well in excess of the CMC there does not appear to be a strong variation of μ_s with further increases in concentration.

Surface dilatational viscosity. Typical experimental techniques to probe surface dilatational properties involve interface area changes and include the use of capillary waves,[99] oscillating drops and bubbles,[58,59,100] and the maximum bubble pressure method.[57] For example, in the context of the maximum bubble pressure method,[57] to avoid the contribution from Marangoni effects uniform interface dilation mode (when the bubble expands radially) is used in the measurements, as well as the sorption effects are avoided by rapid expansion of bubbles so that there is essentially no transport of surfactant to the interface.[85]

Kao *et al.*[57] utilized a maximum bubble pressure method to measure surface dilatational viscosity of surfactant solutions spanning a range of concentrations corresponding to values above and below the CMC ($0.01 \lesssim c \lesssim 12$). They found that below the CMC, the value of κ_s increases with increasing concentration, while above the CMC, κ_s decreases with further increase in bulk concentration. Their results agree with the trends reported by Stenvot and Langevin[99] for DTAB surfactant, namely, increase in κ_s with concentration below the CMC and decrease above the CMC. Kao *et al.* commented that κ_s returns to a "negligible" value for systems with a surfactant concentration one order of magnitude above the CMC. A discrepancy was also reported between magnitudes of κ_s for "research-purity" and "industrial-purity" surfactants, the former having the larger of the measured values of κ_s. Over the entire range of concentrations tested, the dilation viscosity was reported to vary between around 10^{-9} and 10^{-7} Pa s m. Typical magnitudes of κ_s for SDS concentrations near the CMC are also on the order of $10^{-8} - 10^{-7}$ Pa s m. More recently, Fruhner *et al.*[58] and Wantke *et al.*[59] used an oscillating bubble method to measure surface dilatational modulus (from which κ_s can be obtained) for SDS solutions below the CMC with the majority of their reported values falling within the $10^{-6} - 10^{-5}$ Pa s m range. Inspection of the reported values in those works suggests that there appears to be an increase in magnitude of κ_s with surfactant bulk concentration, with values of "approximately zero"[58] for concentrations well below the CMC.

From this diverse group of experiments it is apparent then that the surface dilatational viscosity is a function of the surfactant bulk concentration, with increasing values of κ_s below the CMC and decreasing values above (cf. Figure 16(b)). However, there exists a large degree of variation in the reported values for any particular surfactant concentration. This wide range of differences in values may be related to deformation rate dependence of the surface viscosity, as expansion rates can vary considerably for different experimental methods.[85]

Summary: Range of values for $\mu_s(c)$ and $\kappa_s(c)$. From reviewing the literature we have found that even a well characterized surfactant such a SDS has a wide range of reported values of both μ_s and κ_s for the surfactant concentrations relevant to our experiments ($0.25 < c < 5.0$). Because of this, natural scatter due to experimental accuracy, and availability of data not for all exact concentrations used in our experiments but in their neighborhood, we can only report *ranges of values*, which suffices for our purpose of estimating the orders of magnitude of surface viscosities. Thus, using all of the surface viscosity data compiled from the literature and shown in Figures 16(a) and 16(b), by rounding to the nearest decade or half decade one can compile a range of values of μ_s and κ_s for each of the SDS bulk concentrations in Table I.

Furthermore, we can overlay the data from Figures 16(a) and 16(b) to compare directly the magnitudes of μ_s and κ_s for the range of concentrations relevant in our experiments. This is provided in Figure 17 where a shaded region highlights our concentration range of interest.

By inspection of Figure 17 it is apparent that at low surfactant concentrations (below the CMC), both shear viscosity and dilatational viscosity tend to increase with concentration. Despite the scatter, it is noticeable that many of the dilatational viscosity values are in excess of those for shear viscosity.

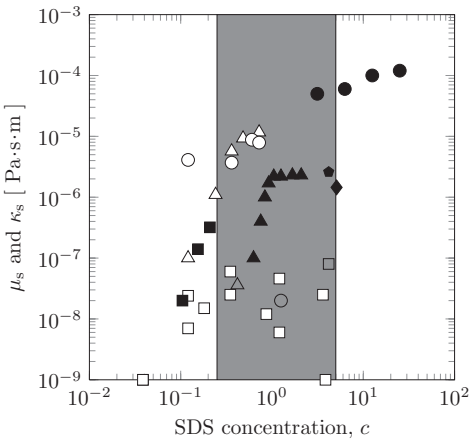

FIG. 17. Measured values of surface dilatational κ_s (empty symbols) and surface shear μ_s (filled symbols) viscosities as functions of the SDS surfactant concentration. The CMC concentration is denoted by the bold dashed line. Concentrations explored in the flow visualization experiments reported here (i.e., $0.25 \leq c \leq 5.0$) fall into the range indicated by the shaded gray region.

This can also be seen by comparing the upper limit of the ranges of μ_s and κ_s for $c = 0.25$ and $c = 0.50$ in Table I. However, for larger values of SDS concentrations (above the CMC), the values for shear viscosity essentially level off while those for the dilatational viscosity decrease dramatically. Again, this is supported by the upper limit of the magnitude ranges in Table I.

[1] S. F. Kistler and P. M. Schweizer, *Liquid Film Coating: Scientific Principles and Their Technological Implications* (Chapman and Hall, London, 1997).
[2] P. Groenveld, "Dip-coating by withdrawal of liquid films," Ph.D. dissertation (Delft University, 1970).
[3] L. Landau and B. Levich, "Dragging of a liquid by a moving plate," Acta Physicochim. URSS **17**, 42–54 (1942).
[4] R. Krechetnikov, "On application of lubrication approximations to nonunidirectional coating flows with clean and surfactant interfaces," Phys. Fluids **22**, 092102 (2010).
[5] C. Y. Lee and J. A. Tallmadge, "The stagnation point in free coating," AIChE J. **19**, 865–866 (1973).
[6] B. Deryagin and A. Titievskaya, "Experimental study of liquid film thickness left on a solid wall after receding meniscus," Dokl. Akad. Nauk SSSR **50**, 307–310 (1945).
[7] F. P. Bretherton, "The motion of long bubbles in tubes," J. Fluid Mech. **10**, 166–189 (1961).
[8] K. J. Mysels, K. Shinoda, and S. Frankel, *Soap Films – Studies of Their Thinning* (Pergamon, New York, 1959).
[9] R. Krechetnikov and G. M. Homsy, "Surfactant effects in the Landau-Levich problem," J. Fluid Mech. **559**, 429–450 (2006).
[10] A. de Ryck and D. Quéré, "Gravity and inertia effects in plate coating," J. Colloid Interface Sci. **203**, 278–285 (1998).
[11] J. A. Tallmadge and A. J. Soroka, "The additional parameter in withdrawal," Chem. Eng. Sci. **24**, 377–383 (1969).
[12] P. Groenveld, "Laminar withdrawal with appreciable inertial forces," Chem. Eng. Sci. **25**, 1267–1273 (1970).
[13] J. A. Tallmadge and R. Stella, "Some properties of the apparent water paradox in entrainment," AIChE J. **14**, 838–840 (1968).
[14] R. R. Stella, "The water paradox," M.S. thesis (Drexel Institute of Technology, 1968).
[15] An early example of film thickening, believed to be the result of surface charge and cleaning procedures, was deemed the "*water paradox*" by its discoverers (Tallmadge and White).
[16] P. Groenveld, "Low capillary number withdrawal," Chem. Eng. Sci. **25**, 1259–1266 (1970).
[17] O. O. Ramdane and D. Quéré, "Thickening factor in Marangoni coating," Langmuir **13**, 2911–2916 (1997).
[18] D. Quéré, A. de Ryck, and O. O. Ramdane, "Liquid coating from a surfactant solution," Europhys. Lett. **37**, 305–310 (1997).
[19] A. Q. Shen, B. Gleason, G. H. McKinley, and H. A. Stone, "Fiber coating with surfactant solutions," Phys. Fluids **14**, 4055–4068 (2002).
[20] R. Krechetnikov and G. M. Homsy, "Experimental study of substrate roughness and surfactant effects on the Landau-Levich law," Phys. Fluids **17**, 102108 (2005).
[21] E. Rame, "The stagnation point in Marangoni-thickened Landau-Levich type flows," Phys. Fluids **19**, 078102 (2007).
[22] B. Scheid, J. Delacotte, B. Dollet, E. Rio, F. Restagno, E. A. V. Nierop, I. Cantat, D. Langevin, and H. A. Stone, "The role of surface rheology in liquid film formation," Europhys. Lett. **90**, 24002 (2010).
[23] D. M. Campana, S. Ubal, M. D. Giavedoni, and F. A. Saita, "Numerical prediction of the film thickening due to surfactants in the Landau-Levich problem," Phys. Fluids **22**, 032103 (2010).

[24] K. J. Ruschak, "Coating flows," Ann. Rev. Fluid Mech. **17**, 65–89 (1985).
[25] S. J. Weinstein and K. J. Ruschak, "Coating flows," Ann. Rev. Fluid Mech. **36**, 29–53 (2004).
[26] D. Quéré, "Fluid coating on a fiber," Ann. Rev. Fluid Mech. **31**, 347–384 (1999).
[27] F. S. Goucher and H. Ward, "A problem of viscosity: the thickness of liquid films formed on solid surfaces under dynamic conditions," Philos. Mag. **XLIV**, 1002–1014 (1922).
[28] V. Stott, "Notes on burettes," J. Soc. Glass Tech. **VII**, 169–198 (1923).
[29] F. C. Morey, "Thickness of a liquid film adhering to surface slowly withdrawn from the liquid," J. Res. Nat. Bur. Stand. **25**, 385–393 (1940).
[30] J. J. van Rossum, "Viscous lifting and drainage of liquids," Appl. Sci. Res., Sec. A **7**, 121–144 (1958).
[31] J. A. Tallmadge and C. Gutfinger, "Entrainment of liquid films. Drainage, withdrawal and removal," Ind. Eng. Chem. **59**, 19–34 (1967).
[32] R. N. Marchessault and S. G. Mason, "Flow of entrapped bubbles through a capillary," Ind. Eng. Chem. **52**, 79–84 (1960).
[33] D. A. White, "Films of Newtonian liquids on cylinders," Ph.D. dissertation (Yale University, 1965).
[34] J. A. Tallmadge, "Prediction of rinsing performance for design purposes," in *Proceedings of the 11th Ontario Industrial Waste Conference* (Ontario Water Resources Commission, Ontario, 1964), pp. 121–136.
[35] D. A. White and J. A. Tallmadge, "Theory of drag out of liquids on flat plates," Chem. Eng. Sci. **20**, 33–37 (1965).
[36] R. Krechetnikov and G. M. Homsy, "Dip coating in the presence of substrate-liquid interaction potential," Phys. Fluids **17**, 102105 (2005).
[37] The measurability of the film thickness with gravimetric technique (Ref. 20) is related to the lifetime of the film. When the film is destroyed by a film instability, it will rupture and dewetting can cause part of the film mass to flow back into the bath, thereby influencing the measurement of film thickness based on mass flux calculations.
[38] P. Groenveld, "High capillary number withdrawal from viscous Newtonian liquids by flat plates," Chem. Eng. Sci. **25**, 33–40 (1970).
[39] P. Groenveld, "Withdrawal of power law fluid films," Chem. Eng. Sci. **25**, 1579–1585 (1970).
[40] P. Groenveld and R. A. V. Dortmund, "The shape of the air interface during the formation of viscous liquid films by withdrawal," Chem. Eng. Sci. **25**, 1571–1578 (1970).
[41] B. J. Carroll and J. Lucassen, "Capillarity-controlled entrainment of liquid by a thin cylindrical filament moving through an interface," Chem. Eng. Sci. **28**, 23–30 (1973).
[42] K. J. Stebe, S. Lin, and C. Maldarelli, "Remobilizing surfactant retarded fluid particle interfaces. I. Stress-free conditions at the interfaces of micellar solutions of surfactants with fast sorption kinetics," Phys. Fluids A **3**, 3–20 (1991).
[43] M. J. Savelski, S. A. Shetty, W. B. Kolb, and R. L. Cerro, "Flow patterns associated with steady movement of a solid/liquid/fluid contact line," J. Colloid Interface Sci. **176**, 117–127 (1995).
[44] J. Fuentes and R. L. Cerro, "Flow patterns and interfacial velocities near a moving contact line," Exp. Fluids **38**, 503–510 (2005).
[45] J. P. Kizito, Y. Kamotani, and S. Ostrach, "Experimental free coating flows at high capillary and Reynolds number," Exp. Fluids **27**, 235–243 (1999).
[46] C.-W. Chen and T.-J. Liu, "Maximum withdrawal speed for Langmuir-Blodgett film deposition of arachidic acid," J. Colloid Interface Sci. **298**, 298–305 (2006).
[47] C. Y. Lee and J. A. Tallmadge, "Meniscus vortexing in free coating," AIChE J. **18**, 858–860 (1972).
[48] R. L. Cerro, "Moving contact lines and Langmuir-Blodgett film deposition," J. Colloid Interface Sci. **257**, 276–283 (2003).
[49] The magnitude of the surface roughness is less than the smallest estimated film thickness. It should be emphasized that the flow patterns reported on in Sec. IV were observed for both the roughened plates at low surfactant concentration (0.25 CMC) and the smooth plates for all higher concentrations. Therefore, the roughness of the plate cannot be the cause of the observed flow patterns.
[50] Fluid acceleration normal to the substrate can also be thought of in terms of a flat plate withdrawn from a bath at some angle from the surface. In this case, a component of gravity is normal to the substrate and results in a deviation from the Landau-Levich law [see S. D. R. Wilson, "The drag-out problem in film coating theory," J. Eng. Math. **16**, 209–221 (1982)].
[51] As indicated earlier, the flow field as shown in Figure 2 was influenced by the nature of the return flow into the small tank. To ensure that the compensating plate had no effect on the observed patterns, several experiments were performed without it. These exhibited the same patterns; however, without the compensating plate the surface level would drop by $\sim$3 mm. This made adequate imaging of the flow field impossible with the stationary camera.
[52] B. P. Binks, "Particles as surfactants – similarities and differences," Curr. Opin. Colloid Interface Sci. **7**, 21–41 (2002).
[53] T. Okubo, "Surface tension of structured colloidal suspensions of polystyrene and silica spheres at the air-water interface," J. Colloid Interface Sci. **171**, 55–62 (1995).
[54] J. C. T. Kao, A. L. Blakemore, and A. E. Hosoi, "Pulling bubbles from a bath," Phys. Fluids **22**, 061705 (2010).
[55] *CRC Handbook of Chemistry and Physics* (Taylor & Francis, Boca Raton, 2007).
[56] K. Tajima, M. Muramatsu, and T. Sakaki, "Radiotracer studies on adsorption of surface active substance at aqueous surface. I. Accurate measurements of adsorption of tritiated sodium dodecylsulfate," Bull. Chem. Soc. Jpn. **43**, 1991–1998 (1970).
[57] R. L. Kao, D. A. Edwards, D. T. Wasan, and E. Chen, "Measurement of interfacial dilatational viscosity at high rates of interface expansion using the maximum bubble pressure method. I. Gas-liquid surface," J. Colloid Interface Sci. **148**, 247–256 (1992).
[58] H. Fruhner, K. D. Wantke, and K. Lunkenheimer, "Relationship between surface dilational properties and foam stability," Colloids Surf., A **162**, 193–202 (1999).

[59] K. D. Wantke, H. Fruhner, and J. Örtegren, "Surface dilatational properties of mixed sodium dodecyl sulfate/dodecanol solutions," Colloids Surf., A **221**, 185–195 (2003).
[60] P. A. Harvey, A. V. Nguyen, G. J. Jameson, and G. M. Evans, "Influence of sodium dodecyl sulphate and Dowfroth frothers on froth stability," Minerals Eng. **18**, 311–315 (2005).
[61] A. Patist, T. Axelberd, and D. Shah, "Effect of long chain alcohols on micellar relaxation time and foaming properties of sodium dodecyl sulfate solutions," J. Colloid Interface Sci. **208**, 259–265 (1998).
[62] A. M. Poskanzer and F. C. Goodrich, "Surface viscosity of sodium dodecyl sulfate solutions with and without added dodecanol," J. Phys. Chem. **79**, 2122–2126 (1975).
[63] C. Barentin, C. Ybert, J. Meglio, and J. Joanny, "Surface shear viscosity of Gibbs and Langmuir monolayers," J. Fluid Mech. **397**, 331–349 (1999).
[64] J. T. Petkov, K. D. Danov, N. D. Denkov, R. Aust, and F. Durst, "Precise method for measuring the shear surface viscosity of surfactant monolayers," Langmuir **12**, 2650–2653 (1996).
[65] S. A. Koehler, S. Hilgenfeldt, E. R. Weeks, and H. A. Stone, "Drainage of single Plateau borders: direct observation of rigid and mobile interfaces," Phys. Rev. E **66**, 040601 (2002).
[66] O. Pitois, C. Fritz, and M. Vignes-Alder, "Liquid drainage through aqueous foam: study of the flow on the bubble scale," J. Colloid Interface Sci. **282**, 458–465 (2005).
[67] A. Saint-Jalmes, Y. Zhang, and D. Langevin, "Quantitative description of foam drainage: transitions with surface mobility," Eur. Phys. J. E **15**, 53–60 (2004).
[68] C. Chang and E. I. Franses, "Adsorption dynamics of surfactants at the air-water interface: a critical review of mathematical models, data, and mechanisms," Colloids Surf., A **100**, 1–45 (1995).
[69] J. Fernandez, R. Krechetnikov, and G. M. Homsy, "Experimental study of a surfactant-driven fingering phenomenon in a Hele-Shaw cell," J. Fluid Mech. **527**, 197–216 (2005).
[70] The complete data set used by Fernandez *et al.* (Ref. 69) can be found in the surfactant adsorption dynamics review article by Chang and Franses (Ref. 68). This reference contains values for k_a^* and k_d^* at four bulk concentrations (none of which corresponds exactly to those used in our experiments) that can be used in the modified Langmuir-Hinshelwood equation:

$$\frac{d\Gamma}{dt} = k_a^* C(1-\theta)e^{-B\theta} - k_d^* \Gamma e^{-B\theta},$$

which differs from L-H by the empirical constant B, amounted to an activation energy barrier concept. This model allows a better fit to the data, but at the expense of having all constants k_a^*, k_d^*, and B as functions of the bulk concentration C. In order to determine values for the adsorption k_a^* and desorption k_d^* rate constants for the specific SDS concentrations tested in our experiments, one would need to interpolate not only k_a^* and k_d^*, but also an empirical exponential parameter B. As interpolation using a small number of data points is undesirable, especially given the large exponential parameter B, the conditionally averaged value reported in Table II is considered more reliable and consistent (in the order of magnitude) with previous estimates based on the standard Langmuir-Hinshelwood model [see C. Chang and E. I. Franses, "Modified Langmuir-Hinshelwood kinetics for dynamic adsorption of surfactants at the air/water interface," Colloids Surf. **69**, 189–201 (1992)].
[71] C. Y. Lee and J. A. Tallmadge, "Description of the meniscus profile in free coating," AIChE J. **18**, 1077–1079 (1972).
[72] M. Maleki, M. Reyssat, F. Restagno, D. Quéré, and C. Clanet, "Landau-Levich menisci," J. Colloid Interface Sci. **354**, 359–363 (2011).
[73] Measurements of the acceleration and deceleration of the stepper motor/lead screw assembly suggest a value of $\sim$20 cm/s^2. Therefore, the faster the prescribed withdrawal speed the longer the start up time, which ranges from $\sim$0.05 to $\sim$0.3 s. These times are a small fraction of the total run times of the experiments.
[74] H. Schlichting, *Boundary-Layer Theory* (McGraw-Hill, New York, 1968).
[75] C. Huh and L. E. Scriven, "Hydrodynamic model of steady movement of a solid/liquid/fluid contact line," J. Colloid Interface Sci. **35**, 85–101 (1970).
[76] This is due to the rather aggressive nature of the air-water interface to adsorb impurities, which in turn is the result of the potential drop ($\sim$0.25 V) across the interface as first measured by Frumkin.
[77] D. M. Henderson, H. Segur, and J. D. Carter, "Experimental evidence of stable wave patterns on deep water," J. Fluid Mech. **658**, 247–278 (2010).
[78] An alternate definition for the Landau number is given as $La = Re_{l_c} Ca$, where Re_{l_c} is based on the capillary length l_c.
[79] J. Ratulowski and H.-C. Chang, "Marangoni effects of trace impurities on the motion of long gas bubbles in capillarities," J. Fluid Mech. **210**, 303–328 (1990).
[80] C.-W. Park, "Effects of insoluble surfactants on dip coating," J. Colloid Interface Sci. **146**, 382–394 (1991).
[81] G. M. Ginley and C. J. Radke, "Influence of soluble surfactants on the flow of long bubbles through a cylindrical capillary," ACS Symp. Ser. **396**, 480–501 (1989).
[82] The authors believe that Groenveld's analysis (Refs. 2 and 16) of the effect of surface impurities is the first instance where the $4^{2/3}$ thickening factor is derived. However, this maximum thickening factor has not been attributed to him perhaps due to a printed error in his publications. For the case of a rigidly moving interface – where the velocity of the interface is of the same value as the substrate – Eq. (27) in his work (Ref. 16) provides a non-dimensional thickness as $2.6Ca^{1/6}$. This can be written in a manner similar to Eq. (2) of this publication, $\overline{h}_\infty = 2.6 l_c Ca^{2/3}$. After review of the procedure with which Eq. (27) was obtained by Groenveld (Ref. 16), it is apparent that the coefficient reported there as 2.6 should be equal to a value of 2.376. If we use the thickening factor commonly defined by Eq. (3) in this paper, then Groenveld's corrected Eq. (27) could be written as $\overline{h}_\infty = \alpha 0.945 l_c Ca^{2/3}$. Thus, $2.376 = \alpha \times 0.945$, and $\alpha = 2.514 \simeq 4^{2/3}$.
[83] The limiting interfacial velocity in the bubble cap region, u_{lim}^σ in the notation of RC, is the velocity of the interface as the bubble cap region is *approached* from the transition region. For the Bretherton case (clean interface), $u_{\text{lim}}^\sigma = 0.5$. Inspection of Figure 7 in RC (Ref. 79) shows that for any of the surfactant-laden cases, there exists a range of capillary

numbers for which u^{σ}_{lim} is negative. This is the same sign as that of the surface velocity in the thin film region, where surface velocity $u^{\sigma} = -1$ (again in the notation of RC), which requires that no surface stagnation point can exists between the thin film region and the bubble cap region.

[84] The choice of Marangoni numbers was based on a reported range of $10^{-2} < M < 10^{2}$ for a condensed monolayer of stearic acid on water.

[85] D. A. Edwards, H. Brenner, and D. T. Wasan, *Interfacial Transport Processes and Rheology* (Butterworth, Boston, 1991).

[86] S. Naire, R. J. Braun, and S. A. Snow, "An insoluble surfactant model for a vertical draining free film with variable surface viscosity," Phys. Fluids **13**, 2492–2502 (2001).

[87] E. A. V. Nierop, B. Scheid, and H. A. Stone, "On the thickness of soap films: an alternative to Frankel's law," J. Fluid Mech. **602**, 119–127 (2008).

[88] A. W. Adamson and A. P. Gast, *Physical Chemistry of Surfaces* (Wiley, New York, 1997).

[89] Note that we discuss the effects of both surface shear and dilatational viscosities in the context of the models accepted in the literature, e.g., Eq. (6) in Naire *et al.* (Ref. 86), Eq. (A2) in van Nierop *et al.* (Ref. 87), and Eqs. (5) and (6) in Naire *et al.* [see S. Naire, R. J. Braun, and S. A. Snow, "A 2+1 dimensional insoluble surfactant model for a vertical draining free film," J. Comput. Appl. Math. **166**, 385–410 (2004)]. The common feature of these models for a one-dimensional interface, as in the considered Landau-Levich problem, is that the surface viscosity effects appear as a sum of both surface shear and dilatational contributions. While it is true that in such a limit, at least for flat interfaces (Ref. 85), the Boussinesq-Scriven model gives the term $(\kappa_s + \mu_s)u_{xx}$ as shown in Eq. (8), intuitively it does not conform with the physical definition of surface shear viscosity as arising due to the shear of the surface velocity field on a two-dimensional interface [see Ref. 85 and M. V. Den Tempel, "Surface rheology," J. Non-Newtonian Fluid Mech. **2**, 205–219 (1977)] since there is no surface shear in the case of one-dimensional interfaces.

[90] Note that we used the value of adsorption coefficient from Table I instead of the rough estimate by Ramdane and Quere (Ref. 17) for 10 CMC – our quantity is based on the fit of the modified Langmuir-Hinshelwood kinetics to experimentally measured data [cf. Ref. 70 and C. Chang and E. I. Franses, "Modified Langmuir-Hinshelwood kinetics for dynamic adsorption of surfactants at the air/water interface," Colloids Surf. **69**, 189–201 (1992)] and compares to the previously reported valued in the standard Langmuir-Hinshelwood model [see C. Chang and E. I. Franses, "Modified Langmuir-Hinshelwood kinetics for dynamic adsorption of surfactants at the air/water interface," Colloids Surf. **69**, 189–201 (1992)].

[91] S.-G. Oh and D. O. Shah, "Relationship between micellar lifetime and foamability of sodium dodecyl sulfate and sodium dodecyl sulfate/1-hexanol mixtures," Langmuir **7**, 1316–1318 (1991).

[92] In order to evaluate the elasticity number, one needs $\mathrm{d}\sigma/\mathrm{d}\Gamma = (\mathrm{d}\sigma/\mathrm{d}C)(\mathrm{d}C/\mathrm{d}\Gamma)$. While $\mathrm{d}\sigma/\mathrm{d}C$ can be easily evaluated from experimental measurements, e.g., Figure 1 of Elworthy and Mysels [see P. H. Elworthy and K. J. Mysels, "The surface tension of sodium deodecylsulfate solutions and the phase separation model of micelle formation," J. Colloid Interface Sci. **21**, 331–347 (1966)]. $\mathrm{d}C/\mathrm{d}\Gamma$ appears to be infinite from Figure 5 in Tajima *et al.* (Ref. 56). Therefore, the possibility of non-zero Marangoni number cannot be excluded. Also, some empirical state equations, such as Sheludko's equation [see B. D. Edmonstone, R. V. Craster, and O. K. Matar, "Surfactant-induced fingering phenomena beyond the critical micelle concentration," J. Fluid Mech. **564**, 105–138 (2006)], give non-zero values of the Marangoni number when applied above CMC, though their validity for SDS solutions has not been verified.

[93] H. K. Moffatt, "Viscous and resistive eddies near a sharp corner," J. Fluid Mech. **18**, 1–18 (1964).

[94] The flow field for the surfactant-laden case from Campana *et al.* (Ref. 23) is similar to the sketch in Figure 1(c) (not to scale). The pattern is one of a homoclinic connection encircling a vortex. This is clearly structurally unstable. To understand this one can draw upon the analogy with the phase flow of a simple gravity pendulum, which is structurally unstable as demonstrated by the unfolding procedure: any generic perturbations will destroy the topology of the phase portrait. Thus, the flow field of Campana *et al.* (Ref. 23) cannot be realized in practice.

[95] D. W. Fallest, A. M. Lichtenberger, C. J. Fox, and K. E. Daniels, "Fluorescent visualization of spreading surfactant," New J. Phys. **12**, 073029 (2010).

[96] An example of an excluded set of published surface viscosity data is that of Liu and Duncan [see X. Liu and J. H. Duncan, "An experimental study of surfactant effects on spilling breakers," J. Fluid Mech. **567**, 433–455 (2006) and X. Liu and J. H. Duncan, "The effects of surfactants on spilling breaking waves," Nature (London) **421**, 520–523 (2003)]. In those works, surface viscosity data are provided for a range of bulk concentrations between $\sim 0.002 < c < \sim 0.05$. This is *well outside* the range of SDS concentrations utilized in our experiments. Liu and Duncan report values of surface viscosity, measured with a capillary wave technique, that vary between $\sim 2 \times 10^{-3}$ and $\sim 5 \times 10^{-4}$Pa s m with a decrease in surface viscosity with increasing concentration. This is in contradiction to established trends for concentrations below the CMC (Ref. 85) that predict an increase in surface viscosity (either shear or dilatational) with concentration. Finally, Liu and Duncan [see X. Liu and J. H. Duncan, "The effects of surfactants on spilling breaking waves," Nature (London) **421**, 520–523 (2003)] state that the values of surface viscosity are measurements of "the sum of the surface shear and dilatational viscosities." As none of our criteria for literature data selection are met, the reported values of Liue and Duncan are excluded from further consideration.

[97] P. Stevenson, "Remarks on the shear viscosity of surfaces stabilised with soluble surfactants," J. Colloid Interface Sci. **290**, 603–606 (2005).

[98] The review article of Stevenson (Ref. 97) contains two more values for the surface shear viscosity. However, these values are provided without a SDS bulk concentration and so they have not been included here.

[99] C. Stenvot and D. Langevin, "Study of viscoelasticity of soluble monolayers using analysis of propagation of excited capillary waves," Langmuir **4**, 1179–1183 (1988).

[100] B. Warburton, "Interfacial rheology," Curr. Opin. Colloid Interface Sci. **1**, 481–486 (1996).